National Physical Laboratory

NPL REPORT ENG 36

Determination of the transfer function for optical surface topography measuring instruments

M R Foreman, C L Giusca, and R K Leach,
Engineering Measurement Division
National Physical Laboratory

J M Coupland
Wolfson School of Mechanical and Manufacturing Engineering
University of Loughborough

JULY 2012

National
Measurement
System

NPL Report ENG 36

Determination of the transfer function for optical surface topography measuring instruments

M R Foreman, C L Giusca, and R K Leach,
Engineering Measurement Division
National Physical Laboratory

J M Coupland
Wolfson School of Mechanical and Manufacturing Engineering
University of Loughborough

July 30, 2012

ABSTRACT

A significant number of areal surface topography measuring instruments, largely based on optical techniques, are commercially available. However, implementation of optical instrumentation into production is problematic due to the lack of understanding of the complex interaction between the light and the component surface - studying the optical transfer function of the instrument could help address this issue. The purpose of this report is to review optical transfer function measurement techniques. Starting from the basis of a spatially coherent, monochromatic confocal scanning imaging system, the theory of optical transfer functions in three dimensional (3D) imaging is presented. Further generalisations are reviewed allowing extension of the theory to the description of conventional and interferometric 3D imaging systems, over a range of spatial coherence. Polychromatic transfer functions are also briefly considered. Specialisation to the measurement of surface topography is further made. Following presentation of theoretical results, experimental methods to measure the optical transfer function of each class of system are presented, with a focus on suitable methods for establishment of calibration standards in 3D imaging and surface topography measurements.

NPL Report ENG 36

ISSN 1754–2987

First issued: July 30, 2012

National Physical Laboratory,
Hampton Road, Teddington, Middlesex, United Kingdom TW11 0LW

This work was funded by the BIS National Measurement System Engineering Measurement Programme 2011–2014 and the EPSRC Knowledge Transfer Secondment scheme 2011. We also thank Rahul Mandal and Kanik Palodhi (University of Loughborough, UK), and Prof. Peter Török (Imperial College London, UK) for their contributions.

Approved on behalf of NPLML by Andrew Lewis,
Science Area Leader, Dimensional Metrology

Contents

List of Figures

1 Introduction

The performance and functional properties of a large number of engineered surfaces and parts can depend strongly on the topographical and textural characteristics. For example, surface deviations in ground optical lenses can give rise to optical aberrations degrading imaging quality, whilst roughness in engine parts can lead to increased wear and shorter component lifetimes. Accordingly, determination of surface properties has long been an important problem since this can play a crucial role in controlling manufacturing procedures and allowing quality control of components such as MEMS wafers, industrial coatings, optical lenses and machined parts. Furthermore, in many situations information gained from surface topography data allows development of new product specifications with enhanced functionality.

Historically, a number of complementary techniques have been employed to perform surface topography measurements, namely stylus and optical probe based instruments [1, 2]. Mechanical stylus based instruments were initially exclusively used to measure height variations with high resolution, whilst optical methods were oriented towards measurement of transverse structure. However, as these techniques have developed so their capabilities and three-dimensional (3D) and areal capabilities have converged in the so called “horns of metrology” [3]. Greater demands are, however, being made of surface metrology particularly at nanometre scales, where high resolution and rapid data acquisition is sought. Optical techniques, such as conventional Michelson and Twyman-Green interferometry [4], Schmaltz light sectioning microscopy [5], Tolansky multiple beam interferometry [6], fringes of equal chromatic order (FECO) interferometry [7], Linnik microinterferometry [8], Mirau interferometry [9], phase shifting interferometry [10], coherence scanning/white light interferometry [11, 12] and confocal microscopy [13], have the potential to satisfy these needs.

Crucial to the establishment and uptake of such metrology techniques is a framework for instrument calibration, allowing traceability back to the definition of the metre. Furthermore, measurement standards are also required for the various optical techniques currently employed. A series of documents describing the nominal characteristics of, and calibration methods for, the scales of areal surface topography measuring instruments are currently under development as part of international standardisation effort in the field of areal surface topography measurement. In line with the standardisation effort, a number of calibration protocols and evaluation techniques have been developed at NPL, for example those detailed in [14, 15, 16], using bespoke primary instrumentation [17, 18], however, they address only the calibration of the scales of an areal surface topography measuring instrument. The calibration consists of measuring the noise and flatness of the instrument, amplification coefficients, linearity and squareness of the scales. Measurement of the optical transfer function of the system provides complete information as to the imaging and measurement properties of an instrument, however, and is, for this reason, being actively pursued [19, 20]. No standard measurement technique has, however, been agreed to date. This report focuses on reviewing work done to date on measuring the optical transfer function as a basis from which to build such a standard.

In this context Section 2 discusses the basics of linear optical theory in which the optical transfer functions of common 3D imaging architectures are defined and discussed. Section 3 proceeds to discuss techniques reported in the literature of how optical transfer functions can, and have, been measured in practice. A concluding discussion is given in Section 4.

2 Three dimensional linear theory in optical metrology

Any measurement system can be regarded as a mathematical mapping from a set of input functions to an associated set of output functions. The system output can thus be represented as $v(\mathbf{r}) = M[u(\mathbf{r}')]$, where $\mathbf{r}$ and $\mathbf{r}'$ are coordinates in output and input space respectively, and $M[\cdots]$ represents the mapping from $u(\mathbf{r}')$ to $v(\mathbf{r})$.

A common approximation in many systems is to assume that the function $M[\cdots]$ is linear, such that the principle of superposition holds. Accordingly if the input function is represented as a superposition of point like elements

$$u(\mathbf{r}') = \int_{V'} u(\mathbf{s})\delta(\mathbf{r}' - \mathbf{s})\, d^3\mathbf{s} \tag{1}$$

where $\mathbf{s}$ is a dummy variable and V' is the domain of the input function, then the measurement output is given by

$$v(\mathbf{r}) = \int_{V'} u(\mathbf{s})M[\delta(\mathbf{r}' - \mathbf{s})]\, d^3\mathbf{s} \tag{2}$$

$$= \int_{V'} u(\mathbf{s})h(\mathbf{r}, \mathbf{s})\, d^3\mathbf{s} \tag{3}$$

where $h(\mathbf{r}, \mathbf{s})$ is known as the impulse response of the measurement system or in the case of optical instruments as the point spread function (PSF). Physically the PSF describes the output from a single elementary input. Further assuming the measurement system to be spatially shift-invariant implies the PSF is dependent only on the difference of coordinates such that $h(\mathbf{r}, \mathbf{s}) = h(\mathbf{r} - \mathbf{s})$. It should be noted that there may exist an implicit scaling in the coordinates (*e.g.* as may be associated with the magnification of an imaging setup). Under these assumptions equation (3) can then be expressed as a 3D convolution *viz.*

$$v(\mathbf{r}) = h(\mathbf{r}) \otimes_3 u(\mathbf{r}) = \int_{\infty} u(\mathbf{s})h(\mathbf{r} - \mathbf{s})d^3\mathbf{s} \tag{4}$$

where the integration limits are over all space, such that the function $u(\mathbf{s})$ is now assumed to adopt a zero value outside the domain V'.

Whilst it is insightful and intuitive to analyse a measurement system in terms of its response to point like inputs, an alternative choice of elementary input function commonly considered is that of a sinusoidally varying function. This analysis ultimately dates back to work of Fourier, but was first considered in optical imaging by Duffieux [21] in 1946, following the sine-wave tests of Selwyn [22]. In this vein it is necessary to move from the spatial domain (described by $\mathbf{r}$ and $\mathbf{r}'$) to a spatial frequency domain. A Fourier representation of equation (4) must thus be adopted whereby the 3D spectrum of the source and output distribution can be defined *via* a 3D inverse Fourier transform *viz.*

$$\tilde{v}(\mathbf{m}) = \int_{\infty} v(\mathbf{r}) e^{-2\pi i \mathbf{m}\cdot\mathbf{r}} d^3\mathbf{r} \tag{5}$$

where $\mathbf{m} = (m, n, q)$ is a triplet of spatial frequencies, and

$$\tilde{u}(\mathbf{m}) = \int_{\infty} u(\mathbf{r}) e^{-2\pi i \mathbf{m}\cdot\mathbf{r}} d^3\mathbf{r}. \tag{6}$$

In the Fourier domain the convolution of equation (4) becomes the mathematically simpler product

$$\tilde{v}(\mathbf{m}) = \tilde{h}(\mathbf{m})\tilde{u}(\mathbf{m}) \tag{7}$$

where

$$\tilde{h}(\mathbf{m}) = \int_{\infty} h(\mathbf{r}) e^{-2\pi i \mathbf{m}\cdot\mathbf{r}} d^3\mathbf{r} \tag{8}$$

is the so-called transfer function.

The function $\tilde{h}(\mathbf{m})$ warrants further discussion, particularly in the context of optical metrology. Fundamental to any optical metrology setup is an imaging setup, to which an interferometric detection architecture may additionally be introduced. Much research has been conducted to date on imaging systems and many alternative configurations exist. For example, the fundamental source of light collected from the sample may be coherent (*e.g.* laser illumination), incoherent (*e.g.* tungsten lamp), or even partially coherent. Moreover, the image formation process itself may also fall into any of these three categories (*e.g.* a fibre-optic scanning confocal reflection, fluorescence microscope or conventional microscope respectively [23, 24, 25]). In the former case the transfer function is more specifically referred to as the optical or coherent transfer function (OTF or CTF) which, by virtue of its complex valued nature, describes both the attenuation and phase shift introduced in the image of a sinusoidal field pattern *i.e.* the system is "linear in field". The modulus of the CTF is known as the modulation transfer function (MTF), whilst the argument is termed the phase transfer function (PTF) [26]. An OTF, MTF, and PTF, can be defined analogously for an incoherent case, however, in this case the system is "linear in intensity". Partially coherent systems are inherently more complicated, with image formation no longer describable using an OTF. Instead a so-called transmission cross-coefficient (TCC) [25, 27] must be defined which describes the attenuation and relative phase shift upon imaging *pairs* of spatial frequencies (of the underlying time instantaneous field). It should be noted that it is sometimes possible to define a so-called weak object transfer function (WOTF) in a partially coherent system if scattering from the object can be considered small [23]. Discussion of WOTFs will, however, not be given here.

Given the array of different imaging configurations it seems a somewhat daunting task to analyse all possible imaging configurations. Equivalencies between confocal and conventional arrangements and scanning microscopes of differing geometries have, however, been expounded [28, 29] reducing the number of distinct geometries that need be considered. This equivalence originates from Helmholtz's principle of reversibility. As such, in this document it is only necessary to describe a scanning confocal microscope with either a point, or infinite, intensity sensitive detector for both coherent and incoherent illumination as is done in Sections 2.2 and 2.3 respectively. A finite sized detector, will also be briefly discussed. A description of partially coherent systems will naturally emerge in these discussions. Interferometric arrangements will also be considered and the OTF for the interference image is derived in Section 2.4. Moreover, only reflection geometries are to be considered as this is the usual practice in optical metrology. The equivalencies of each system geometry will be indicated where appropriate. Before proceeding to derive the OTF for these geometries it is first worth considering the nature of the process by which an illuminating field is scattered from a sample of interest, as is discussed in the next section.

2.1 Scattering theory and the Born approximation

Since engineering surfaces are not self-luminous it is necessary to illuminate them with a known field and measure the light subsequently scattered from the object. The standard starting point for a derivation of the scattered field (see *e.g.* [30]) is the scalar wave equation,

$$\nabla^2 E(\mathbf{r}) + k^2 n^2(\mathbf{r}) E(\mathbf{r}) = 0 \tag{9}$$

where $E(\mathbf{r})$ is the complex electric field at position $\mathbf{r}$ in a medium of refractive index $n(\mathbf{r})$, assumed to be monochromatic with time dependence $\exp(-i\omega t)$ and $k = \omega/c = 2\pi/\lambda$ is the associated wavenumber in vacuum. When a field is incident onto an inhomogeneity in the refractive index, a scattered field results. As such the resulting field is a superposition of the original incident field and the scattered field, *i.e.* $E = E_r + E_s$. Hence

$$\nabla^2 (E_r(\mathbf{r}) + E_s(\mathbf{r})) + k^2 n^2(\mathbf{r})(E_r(\mathbf{r}) + E_s(\mathbf{r})) = 0. \tag{10}$$

Noting that E_r is the illumination field that must satisfy the scalar wave equation in the absence of the scattering object *i.e.* $\nabla^2 E_r(\mathbf{r}) + k^2 E_r(\mathbf{r}) = 0$ yields

$$\nabla^2 E_s(\mathbf{r}) + k^2 n^2(\mathbf{r})(E_r(\mathbf{r}) + E_s(\mathbf{r})) - k^2 E_r(\mathbf{r}) = 0. \tag{11}$$

Hence

$$\left(\nabla^2 + k^2\right) E_s(\mathbf{r}) = k^2 \left(1 - n^2(\mathbf{r})\right) (E_r(\mathbf{r}) + E_s(\mathbf{r})). \tag{12}$$

Letting $t(\mathbf{r}) = k^2 \left[n^2(\mathbf{r}) - 1\right]$ be the scattering potential, equation (12) becomes

$$\left(\nabla^2 + k^2\right) E_s(\mathbf{r}) = t(\mathbf{r})(E_r(\mathbf{r}) + E_s(\mathbf{r})). \tag{13}$$

Equation (13) takes the form of a free-space scalar wave equation with source term (or scattering function) $U(\mathbf{r}) = t(\mathbf{r})(E_r(\mathbf{r}) + E_s(\mathbf{r}))$. Accordingly equation (13) can thus be solved using the Green's function satisfying the equation

$$\left(\nabla^2 + k^2\right) G(\mathbf{r}) = -\delta(\mathbf{r}). \tag{14}$$

The negative sign is introduced by definition. It should also be noted that some definitions include an additional factor of 4π, however, this is omitted here and instead incorporated into the Green's function itself. A solution to equation (14) is the well-known free-space Green's function [31]

$$G(\mathbf{r}) = \frac{e^{ik|\mathbf{r}|}}{4\pi|\mathbf{r}|}. \tag{15}$$

The solution to equation (13) hence takes the form

$$E_s(\mathbf{r}) = \int_{-\infty}^{\infty} G(\mathbf{r} - \mathbf{r}')U(\mathbf{r}')d^3\mathbf{r}' \tag{16}$$

$$= G(\mathbf{r}) \otimes_3 U(\mathbf{r}) \tag{17}$$

where $\otimes_3$ again denotes 3D convolution.

In linear optical scattering a further approximation is generally adopted to allow amenable analysis. Specifically the first Born approximation states that the source term $U(\mathbf{r}) = U_r(\mathbf{r}) + U_s(\mathbf{r})$ can be replaced by $U_r(\mathbf{r})$, that is to say that the object scatters weakly such that

$$U(\mathbf{r}) \approx t(\mathbf{r})E_r(\mathbf{r}). \tag{18}$$

Neglecting effects arising from multiple scattering and depletion of the illumination beam is also implicit in making the Born approximation. Accordingly the interaction with the object can be considered as transmission of the illumination field through an apodising (and phase) mask $t(\mathbf{r}) = k^2\left[n^2(\mathbf{r}) - 1\right]$ (or in a reflection geometry, as reflection from a sample with complex reflectivity $t(\mathbf{r})$). This assumption will be seen to allow derivation of the OTF in a number of complex optical systems. A discussion on the validity of adopting the Born approximation can be found in [32].

2.2 Confocal and conventional coherent imaging systems

Optical metrology is in essence a 3D imaging technique, with object parameters, such as surface height or roughness, derived from a 3D image *via* appropriate data processing. Studies in this field were perhaps first initiated by McCutcheon [33], who considered 3D focusing by a simple lens and by Wolf [34], who discussed the use of holographic measurements to determine the 3D refractive index distribution of a semi-transparent scattering object. Both McCutcheon's and Wolf's treatments, however, described 3D imaging theory in a coherent system. The first treatment of incoherent systems was presented by Frieden who developed a 3D transfer function theory [35], by extending the 2D transfer function originally proposed by Duffieux [21]. A partially coherent treatment of image formation was first presented by Hopkins in his seminal work [36], albeit in a 2D manner, with the 3D treatment given by Striebl [25]. Striebl's work was, however, an approximate treatment in which bilinear terms were neglected. Image formation in confocal microscopes has been shown to fall into a class of imaging systems not considered in Hopkin's or Striebl's original work [28]. As such, Sheppard and Mao extended their work to include the bilinear terms and hence allow a more accurate description of imaging in both conventional and confocal arrangements [27]. Formally, 3D imaging can be considered by introduction of defocused pupil functions into existing 2D treatments [37, 38]. As such it is worthwhile to mention the work of Sheppard and Wilson on 2D image formation in scanning microscopy [39, 40, 41, 42]. However, an alternative is to use a full 3D CTF treatment such as that presented in [24, 43, 23, 44, 45, 46, 47, 48] for example. The derivations presented in these works are, however, for ideal systems. Deviations from such ideal circumstances and their effect on the OTF of imaging systems has been considered in [49, 50], for example.

In the remainder of this section the pertinent theory from the above papers is distilled into a derivation of the OTF and TCC for imaging in both confocal and conventional imaging systems. Following from the equivalence theorem presented in [28, 29], both the OTF and TCC will be derived by considering a confocal scanning system with a point detector and infinite incoherent detector respectively.

Consider the setup shown in Figure 1, which shows the basic setup of a confocal imaging setup in reflection mode. A point source is imaged onto the object of interest by means of an objective lens L_1. The light back scattered is then imaged onto a detector by means of the collector lens L_2. It should be noted that naming conventions for these lenses depends on the exact imaging geometry [42]. In practical systems a single lens is used to perform the role of both objective and collector. A 3D image can be built up by scanning the object in both a transverse and axial direction.

The 3D PSF of each lens is given by [29] under a paraxial approximation

$$h_n(\mathbf{r}) = \iint P_n(\zeta, \eta, z) \exp\left[\frac{ik}{d_n}(\zeta x + \eta y)\right] d\zeta d\eta, \tag{19}$$

where $P_n(\zeta, \eta, z)$ is the defocused pupil function of lens L_n given by [28, 42]

$$P_n(\zeta, \eta, z) = P_n(\zeta, \eta) \exp\left[-\frac{ik}{2d_n^2} z(\zeta^2 + \eta^2)\right], \tag{20}$$

$P_n(\zeta, \eta)$ is the 2D pupil function of lens L_n and d_1 and d_2 are the distances from the objective lens to the source and object respectively. The distances d_1 and d_2 are assumed to obey the thin lens law

$$\frac{1}{d_1} + \frac{1}{d_2} = \frac{1}{f} \tag{21}$$

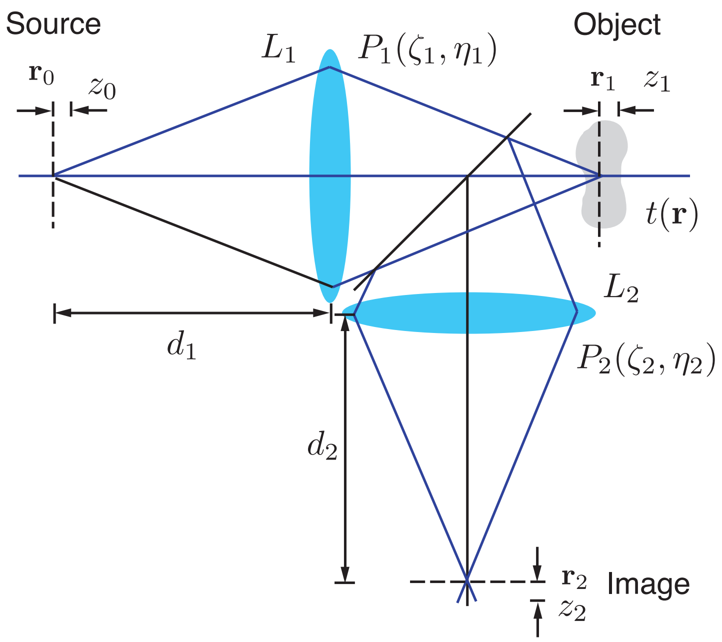

Figure 1: Schematic of the optical setup and coordinate geometry of a reflection type microscope, comprising two lenses L_1 and L_2 with associated pupil functions $P_1(\zeta_1, \eta_1)$ and $P_2(\zeta_2, \eta_2)$. A weakly scattering object is assumed present with scattering properties described by $t(\mathbf{r})$.

where f is the focal length of both L_1 and L_2 as is usual in practice. Note that all limits on integrals will be assumed to be from $-\infty$ to ∞ unless otherwise stated. Whilst here the paraxial approximation has been made, a short discussion of large angle, *i.e.* high numerical aperture (NA) systems, will be given in Section 2.6.

Assuming that the point source is placed at a position $\mathbf{r}_p$, the field incident on the object plane is given by

$$E_r(\mathbf{r}_1) = \int \delta(\mathbf{r}_0 - \mathbf{r}_p) \exp[ik(z_0 - z_1)] h_1(\mathbf{r}_0 + \mathbb{M}_1 \mathbf{r}_1)\, d^3\mathbf{r}_0 \tag{22}$$

$$= \exp[ik(z_p - z_1)] h_1(\mathbf{r}_p + \mathbb{M}_1 \mathbf{r}_1) \tag{23}$$

where, following [29], $\mathbb{M}_1$ is a diagonal 3×3 matrix with diagonal elements $(M_1, M_1, -M_1^2)$ describing the transverse and axial magnifications and $M_1 = d_1/d_2$. The additional phase term $\exp[ik(z_p - z_1)]$ originates from possible axial shifts in the source and object space. Some irrelevant phase factors have been neglected, requiring an implicit assumption that the Fresnel number of the lens is large [29].

From equation (18) the scattering function is then, assuming the object has been scanned to a position $\mathbf{r}_s$, given by

$$U(\mathbf{r}_1, \mathbf{r}_s) \approx t(\mathbf{r}_s - \mathbf{r}_1) \exp[ik(z_p - z_1)] h_1(\mathbf{r}_p + \mathbb{M}_1 \mathbf{r}_1). \tag{24}$$

Following linear imaging theory, the field at a position $\mathbf{r}_2$ in detector space is given by the convolution of the PSF of the collector lens with the source function $U(\mathbf{r}_1, \mathbf{r}_s)$. Treating this field as a function of the object scan position gives

$$\begin{aligned} E_d(\mathbf{r}_s, \mathbf{r}_2, \mathbf{r}_p) &= \int \exp[ik(z_p - z_1)] h_1(\mathbf{r}_p + \mathbb{M}_1 \mathbf{r}_1) \\ &\qquad \times t(\mathbf{r}_s - \mathbf{r}_1) \exp[-ik(z_1 + z_2)] h_2(\mathbf{r}_1 + \mathbb{M}_2 \mathbf{r}_2)\, d^3\mathbf{r}_1 \qquad (25) \\ &= \int \exp[ik(z_p - z_2 - 2z_1)] h_1(\mathbf{r}_p + \mathbb{M}_1 \mathbf{r}_1) h_2(\mathbf{r}_1 + \mathbb{M}_2 \mathbf{r}_2) t(\mathbf{r}_s - \mathbf{r}_1)\, d^3\mathbf{r}_1 \qquad (26) \end{aligned}$$

where $\mathbb{M}_2$ is defined analogously to $\mathbb{M}_1$ with $M_2 = d_2/d_1$ and the signs in the axial phase term account for the fact that a reflection geometry has been assumed. Equation (25) represents the convolution $E_d(\mathbf{r}_s, \mathbf{r}_2, \mathbf{r}_p) = h_{\text{cf}}(\mathbf{r}_s, \mathbf{r}_2, \mathbf{r}_p) \otimes_3 t(\mathbf{r}_s)$, *i.e.* of the scattering potential $t(\mathbf{r}_1)$ with the effective PSF of a confocal reflection mode imaging system [43]

$$h_{\text{cf}}(\mathbf{r}_1, \mathbf{r}_2, \mathbf{r}_p) = \exp[ik(z_p - z_2 - 2z_1)] h_1(\mathbf{r}_p + \mathbb{M}_1 \mathbf{r}_1) h_2(\mathbf{r}_1 + \mathbb{M}_2 \mathbf{r}_2). \tag{27}$$

Moving to a Fourier representation, first consider the 3D spectrum of the scattering function defined by

$$\widetilde{t}(\mathbf{m}) = \int t(\mathbf{r}) \exp[-2\pi i \mathbf{r} \cdot \mathbf{m}]\, d^3\mathbf{r} \tag{28}$$

such that

$$t(\mathbf{r}) = \int \widetilde{t}(\mathbf{m}) \exp[2\pi i \mathbf{r} \cdot \mathbf{m}]\, d^3\mathbf{m}. \tag{29}$$

Substituting equation (29) into equation (25) yields

$$E_d(\mathbf{r}_s, \mathbf{r}_2, \mathbf{r}_p) = \int \widetilde{h}_{\text{cf}}(\mathbf{m}, \mathbf{r}_2, \mathbf{r}_p) \widetilde{t}(\mathbf{m}) \exp[2\pi i \mathbf{r}_s \cdot \mathbf{m}] d^3\mathbf{m} \tag{30}$$

where $\widetilde{h}_{\text{cf}}(\mathbf{m}, \mathbf{r}_2, \mathbf{r}_p)$ is the confocal CTF given by

$$\begin{aligned} \widetilde{h}_{\text{cf}}(\mathbf{m}, \mathbf{r}_2, \mathbf{r}_p) &= \int h_{\text{cf}}(\mathbf{r}_1, \mathbf{r}_2, \mathbf{r}_p) \exp[-2\pi i \mathbf{r}_1 \cdot \mathbf{m}] d^3\mathbf{r}_1 \qquad (31) \\ &= \int \exp[ik(z_p - z_2 - 2z_1)] \\ &\qquad \times h_1(\mathbf{r}_p + \mathbb{M}_1 \mathbf{r}_1) h_2(\mathbf{r}_1 + \mathbb{M}_2 \mathbf{r}_2) \exp[-2\pi i \mathbf{r}_1 \cdot \mathbf{m}] d^3\mathbf{r}_1. \qquad (32) \end{aligned}$$

Substituting equations (19) and (20) in equation (32) gives

$$\widetilde{h}_{\text{cf}}(\mathbf{m}, \mathbf{r}_2, \mathbf{r}_p) = \int \widetilde{h}_{\text{cf}}(m, n, z_1, \mathbf{r}_2, \mathbf{r}_p) \exp[-2\pi i q z_1] dz_1, \tag{33}$$

where $\widetilde{h}_{\text{cf}}(m, n, z_1, \mathbf{r}_2, \mathbf{r}_p)$ is the 2D defocused CTF given by

$$\begin{aligned}
\widetilde{h}_{\text{cf}}(m, n, z_1, \mathbf{r}_2, \mathbf{r}_p) &= \exp[ik(z_p - z_2 - 2z_1)] \\
&\quad \times \int \exp[-2\pi i(mx_1 + ny_1)] h_1(\mathbf{r}_p + \mathbb{M}_1 \mathbf{r}_1) h_2(\mathbf{r}_1 + \mathbb{M}_2 \mathbf{r}_2) dx_1 dy_1 &(34)\\
&= \exp[ik(z_p - z_2 - 2z_1)] \\
&\quad \times \left[\left\{ P_1(\lambda d_2 m, \lambda d_2 n, z_p - M_1^2 z_1) \exp[2\pi i(mx_p + ny_p)] \right\} \right. \\
&\qquad \left. \otimes_2 \left\{ P_2(\lambda d_2 m, \lambda d_2 n, z_1 - M_2^2 z_2) \exp[2\pi i M_2(mx_2 + ny_2)] \right\} \right] &(35)
\end{aligned}$$

where $\otimes_2$ denotes 2D convolution. Explicitly, and in terms of the 2D pupil functions, equation (35) reads

$$\begin{aligned}
\widetilde{h}_{\text{cf}}(m, n, z_1, \mathbf{r}_2, \mathbf{r}_p) &= \exp[ik(z_p - z_2 - 2z_1)] \\
&\times \iint P_1(\zeta, \eta) P_2(m\lambda d_2 - \zeta, n\lambda d_2 - \eta) \exp\left[\frac{ik}{d_1}(\zeta x_p + \eta y_p)\right] \\
&\times \exp\left[\frac{ik}{d_1}(x_2(m\lambda d_2 - \zeta) + y_2(n\lambda d_2 - \eta))\right] \exp\left[-\frac{ik}{2d_1^2}(z_p - M_1^2 z_1)(\zeta^2 + \eta^2)\right] \\
&\times \exp\left[-\frac{ik}{2d_2^2}(z_1 - M_2^2 z_2)((m\lambda d_2 - \zeta)^2 + (n\lambda d_2 - \eta)^2)\right] d\zeta d\eta. \qquad (36)
\end{aligned}$$

Collecting the terms dependent on z_1 together and substituting into equation (33) yields

$$\begin{aligned}
\widetilde{h}_{\text{cf}}(\mathbf{m}, \mathbf{r}_2, \mathbf{r}_p) &= \exp[ik(z_p - z_2)] \\
&\times \iint P_1(\zeta, \eta) P_2(m\lambda d_2 - \zeta, n\lambda d_2 - \eta) \exp\left[\frac{ik}{d_1}(\zeta x_p + \eta y_p)\right] \\
&\times \exp\left[\frac{ik}{d_1}(x_2(m\lambda d_2 - \zeta) + y_2(n\lambda d_2 - \eta))\right] \exp\left[-\frac{ik}{2d_1^2} z_p(\zeta^2 + \eta^2)\right] \\
&\times \exp\left[\frac{ik}{2d_1^2} z_2((m\lambda d_2 - \zeta)^2 + (n\lambda d_2 - \eta)^2)\right] \\
&\times \delta\left(q + \frac{\lambda}{2}(m^2 + n^2) - \frac{1}{d_2}(m\zeta + n\eta) + \frac{2}{\lambda}\right) d\zeta d\eta. \qquad (37)
\end{aligned}$$

For a general finite sized detector described by the response function $D(\mathbf{r}_2)$ the intensity recorded for each scan position is given by

$$I_d(\mathbf{r}_s, \mathbf{r}_p) = \int |E_d(\mathbf{r}_s, \mathbf{r}_2, \mathbf{r}_p)|^2 D(\mathbf{r}_2) d^3\mathbf{r}_2. \tag{38}$$

Working in either the spatial or Fourier domain gives two alternative expressions for this recorded intensity, namely

$$I_d(\mathbf{r}_s, \mathbf{r}_p) = \iint H(\mathbf{r}_1, \mathbf{r}'_1) t(\mathbf{r}_s - \mathbf{r}_1) t^*(\mathbf{r}_s - \mathbf{r}'_1)\, d^3\mathbf{r}_1\, d^3\mathbf{r}'_1 \tag{39}$$

or

$$I_d(\mathbf{r}_s, \mathbf{r}_p) = \iint \widetilde{H}(\mathbf{m}, \mathbf{m}') \widetilde{t}(\mathbf{m}) \widetilde{t}^*(\mathbf{m}') \exp[2\pi i \mathbf{r}_s \cdot (\mathbf{m} - \mathbf{m}')]\, d^3\mathbf{m}\, d^3\mathbf{m}' \tag{40}$$

where

$$H(\mathbf{r}_1, \mathbf{r}'_1) = \int h_{\text{cf}}(\mathbf{r}_1, \mathbf{r}_2, \mathbf{r}_p) h^*_{\text{cf}}(\mathbf{r}'_1, \mathbf{r}_2, \mathbf{r}_p) D(\mathbf{r}_2) d^3\mathbf{r}_2 \tag{41}$$

and

$$\widetilde{H}(\mathbf{m}, \mathbf{m}') = \int \widetilde{h}_{\text{cf}}(\mathbf{m}, \mathbf{r}_2, \mathbf{r}_p) \widetilde{h}^*_{\text{cf}}(\mathbf{m}', \mathbf{r}_2, \mathbf{r}_p) D(\mathbf{r}_2) d^3\mathbf{r}_2. \tag{42}$$

$\widetilde{H}(\mathbf{m}, \mathbf{m}')$ is the TCC introduced above. Considering now the confocal (denoted by the subscript cf) and conventional (cv) cases whereby detection is *via* a point detector at $\mathbf{r}_d$ or by an infinite planar detector at z_d it is evident that

$$D_{\text{cf}}(\mathbf{r}_2) = \delta(\mathbf{r}_2 - \mathbf{r}_d) \tag{43}$$

and

$$D_{\text{cv}}(\mathbf{r}_2) = \delta(z_2 - z_d). \tag{44}$$

For the former case, the sifting property of the Dirac delta function immediately gives the detected intensity as $|E_d(\mathbf{r}_s, \mathbf{r}_d, \mathbf{r}_p)|^2$. Furthermore, earlier expressions for the confocal CTF, such as equations (32) and (37) hold with the simple replacement $\mathbf{r}_2 = \mathbf{r}_d$. For example, for the simple case of an on axis source and detector (*i.e.* $\mathbf{r}_p = \mathbf{r}_d = \mathbf{0}$) the confocal PSF reduces to

$$h_{\text{cf}}(\mathbf{r}_1, \mathbf{0}, \mathbf{0}) = \exp[-2ikz_1] h_1(\mathbb{M}_1 \mathbf{r}_1) h_2(\mathbf{r}_1) \tag{45}$$

and the CTF becomes

$$\begin{aligned} \widetilde{h}_{\text{cf}}(\mathbf{m}, \mathbf{0}, \mathbf{0}) = \iint & P_1(\zeta, \eta) P_2(m\lambda d_2 - \zeta, n\lambda d_2 - \eta) \\ & \times \delta\left(q + \frac{\lambda}{2}(m^2 + n^2) - \frac{1}{d_2}(m\zeta + n\eta) + \frac{2}{\lambda}\right) d\zeta d\eta. \end{aligned} \tag{46}$$

Furthermore, the confocal TCC becomes separable in $\mathbf{m}$ and $\mathbf{m}'$ such that $\widetilde{H}_{\text{cf}}(\mathbf{m}, \mathbf{m}') = \widetilde{h}_{\text{cf}}(\mathbf{m}, \mathbf{0}, \mathbf{0}) \widetilde{h}^*_{\text{cf}}(\mathbf{m}', \mathbf{0}, \mathbf{0})$.

Partial coherence in the image formation in a conventional imaging system implies that the TCC is no longer separable in $\mathbf{m}$ and $\mathbf{m}'$ but is instead given by

$$\widetilde{H}_{\text{cv}}(\mathbf{m},\mathbf{m}') = \iiint \widetilde{h}_{\text{cf}}(\mathbf{m},\mathbf{r}_2,\mathbf{r}_p)\widetilde{h}^*_{\text{cf}}(\mathbf{m}',\mathbf{r}_2,\mathbf{r}_p)\delta(z_2-z_d)dx_2dy_2dz_2 \tag{47}$$

$$\begin{aligned}
&= \iiiint\!\!\iint P_1(\zeta,\eta)P_2(m\lambda d_2-\zeta,n\lambda d_2-\eta)y_p)P_1^*(\zeta',\eta')P_2^*(m'\lambda d_2-\zeta',n'\lambda d_2-\eta') \\
&\quad\times \exp\left[\frac{ik}{d_1}((\zeta-\zeta')x_p+(\eta-\eta')y_p)\right]\exp\left[-\frac{ik}{2d_1^2}z_p(\zeta^2-\zeta^2+\eta^2-\eta^2)\right] \\
&\quad\times \exp\left[\frac{ik}{d_1}(x_2((m-m')\lambda d_2-(\zeta-\zeta'))+y_2((n-n')\lambda d_2-(\eta-\eta')))\right] \\
&\quad\times \exp\left[\frac{ik}{2d_1^2}z_d((m\lambda d_2-\zeta)^2-(m'\lambda d_2-\zeta')^2+(n\lambda d_2-\eta)^2-(n'\lambda d_2-\eta')^2)\right] \\
&\quad\times \delta\left(q+\frac{\lambda}{2}(m^2+n^2)-\frac{1}{d_2}(m\zeta+n\eta)+\frac{2}{\lambda}\right) \\
&\quad\times \delta\left(q'+\frac{\lambda}{2}(m'^2+n'^2)-\frac{1}{d_2}(m'\zeta'+n'\eta')+\frac{2}{\lambda}\right)d\zeta d\eta d\zeta' d\eta' dx_2 dy_2.
\end{aligned} \tag{48}$$

Upon integrating with respect to x_2, y_2, ζ' and η', equation (48) reduces to

$$\begin{aligned}
\widetilde{H}_{\text{cv}}(\mathbf{m},\mathbf{m}') &= \iint P_1(m\lambda d_2-\alpha,n\lambda d_2-\beta)P_1^*(m'\lambda d_2-\alpha,n'\lambda d_2-\beta) \\
&\quad\times |P_2(\alpha,\beta)|^2\exp\left[-\frac{ik}{d_1}((\alpha-\alpha')x_p+(\beta-\beta')y_p)\right] \\
&\quad\times \exp\left[-\frac{ik}{2d_1^2}z_p((m\lambda d_2-\alpha)^2-(m'\lambda d_2-\alpha)^2+(n\lambda d_2-\beta)^2-(n'\lambda d_2-\beta)^2\right] \\
&\quad\times \delta\left(q-\frac{\lambda}{2}(m^2+n^2)+\frac{1}{d_2}(m\alpha+n\beta)+\frac{2}{\lambda}\right) \\
&\quad\times \delta\left(q'-\frac{\lambda}{2}(m'^2+n'^2)+\frac{1}{d_2}(m'\alpha+n'\beta)+\frac{2}{\lambda}\right)d\alpha d\beta
\end{aligned} \tag{49}$$

where a change of variables $\alpha^{(')} = m^{(')}\lambda d_2-\zeta$ and $\beta^{(')} = m^{(')}\lambda d_2-\eta$ has also been made. Note the equivalence between a confocal setup with an infinite detector and a conventional imaging system dictates that the pupil function for the condenser lens in the conventional system is the same as that for the collector in the confocal system and the objective lens in each system is identical [27]. Accordingly in equation (49), P_1 and P_2 refer to the pupil functions of the objective and condenser lens respectively. It is noted that aberrations in the condenser lens are irrelevant with regards to determining the TCC, such that if it is assumed that the condenser is perfectly transmitting, and the source is at $\mathbf{r}_p = \mathbf{0}$, the TCC reduces to

$$\begin{aligned}\widetilde{H}_{\text{cv}}(\mathbf{m},\mathbf{m}') = \iint & P_1(m\lambda d_2-\alpha, n\lambda d_2-\beta)P_1^*(m'\lambda d_2-\alpha, n'\lambda d_2-\beta)\\ &\times\delta\left(q-\frac{\lambda}{2}(m^2+n^2)+\frac{1}{d_2}(m\alpha+n\beta)+\frac{2}{\lambda}\right)\\ &\times\delta\left(q'-\frac{\lambda}{2}(m'^2+n'^2)+\frac{1}{d_2}(m'\alpha+n'\beta)+\frac{2}{\lambda}\right)d\alpha d\beta. \end{aligned} \tag{50}$$

For later reference the image of a point object is briefly considered. For a point object $t(\mathbf{r}) = \delta(\mathbf{r}-\mathbf{r}_o)$ the measured intensity expressed in equation (39) reduces to

$$\begin{aligned} I_d(\mathbf{r}_s,\mathbf{r}_o,\mathbf{r}_p) &= H(\mathbf{r}_s,\mathbf{r}_o,\mathbf{r}_p)\\ &= |h_1(\mathbf{r}_p+\mathbb{M}_1(\mathbf{r}_o+\mathbf{r}_s))|^2\int|h_2((\mathbf{r}_o+\mathbf{r}_s)+\mathbb{M}_2\mathbf{r}_2)|^2\,D(\mathbf{r}_2)\,d^3\mathbf{r}_2 \end{aligned} \tag{51}$$

which is known as the intensity PSF. For a point detector (such as in the ideal confocal case) the intensity PSF is given by

$$H_{\text{cf}}(\mathbf{r}_s,\mathbf{r}_o,\mathbf{r}_p) = |h_1(\mathbf{r}_p+\mathbb{M}_1(\mathbf{r}_o+\mathbf{r}_s))|^2\,|h_2((\mathbf{r}_o+\mathbf{r}_s)+\mathbb{M}_2\mathbf{r}_d)|^2 \tag{52}$$

as would be expected by squaring the amplitude PSF of equation (27). However, for an infinite detector, as is equivalent to a conventional imaging system, equation (51) reduces to

$$H_{\text{cv}}(\mathbf{r}_s,\mathbf{r}_o,\mathbf{r}_p) = |h_1(\mathbf{r}_p+\mathbb{M}_1(\mathbf{r}_o+\mathbf{r}_s))|^2 \tag{53}$$

since convolution with an infinite uniform function has no functional dependence and can be dropped. For zero source and detector offset this reduces to

$$H_{\text{cv}}(\mathbf{r}_s) = |h_1(\mathbb{M}_1\mathbf{r}_s)|^2 \tag{54}$$

A common misconception is that whilst equations (53) and (54) express the image of a point object, equation (39) does not represent the sum of the intensity scattered from each point on an object for a coherent system. This issue will be further discussed in the following section.

2.3 Confocal and conventional incoherent imaging systems

Whilst the preceding section considered image formation in coherent optical systems in which the imaging process acts as a linear filter in field amplitude, incoherent imaging acts as a linear filter in intensity. Incoherent imaging models must be used if, for example, an extended incoherent source is used, or if phase coherence from the illumination field is lost during interaction with the sample, such as in a fluorescence microscope. In optical metrology, the use of an extended incoherent illumination is, by far, the more relevant of these two scenarios. That said, a one photon fluorescence model will be used here [23] and the equivalences detailed in [28] again invoked, such that the imaging geometries adopted thus far (*i.e.* point source) can be maintained and the mathematical framework does not require significant modification.

To begin equation (18) is revisited. Given that phase coherence is assumed to be lost, scattering must be described as a spatially incoherent process whereby

$$I(\mathbf{r}) = T(\mathbf{r}) I_r(\mathbf{r}) \tag{55}$$

where $T(\mathbf{r}) = |t(\mathbf{r})|^2$ and $I_r(\mathbf{r})$ is the illuminating intensity. From equation (23) it follows that

$$I(\mathbf{r}_1, \mathbf{r}_p) = |h_1(\mathbf{r}_p + \mathbb{M}_1 \mathbf{r}_1|^2 T(\mathbf{r}_1) \tag{56}$$

and for an incoherent imaging process the intensity in detector space, for an object scanned to $\mathbf{r}_s$, is given by

$$I_d(\mathbf{r}_s, \mathbf{r}_2, \mathbf{r}_p) = \int |h_1(\mathbf{r}_p + \mathbb{M}_1 \mathbf{r}_1)|^2 |h_2(\mathbf{r}_1 + \mathbb{M}_2 \mathbf{r}_2)|^2 T(\mathbf{r}_s - \mathbf{r}_1) d^3\mathbf{r}_1 \tag{57}$$

in a similar fashion to above. Following earlier discussions the intensity recorded by a finite-sized detector is hence

$$I_d(\mathbf{r}_s, \mathbf{r}_p) = \int H(\mathbf{r}_1, \mathbf{r}_p) T(\mathbf{r}_s - \mathbf{r}_1) d^3\mathbf{r}_1 \tag{58}$$

where now

$$H(\mathbf{r}_1, \mathbf{r}_p) = \int |h_1(\mathbf{r}_p + \mathbb{M}_1 \mathbf{r}_1)|^2 |h_2(\mathbf{r}_1 + \mathbb{M}_2 \mathbf{r}_2)|^2 D(\mathbf{r}_2) d^3\mathbf{r}_2 \tag{59}$$

is again the intensity PSF for a point object at $\mathbf{r}_1$. Restricting to the ideal confocal (point detector) and conventional (infinite detector) case gives

$$H_{\text{cf}}(\mathbf{r}_s, \mathbf{r}_o, \mathbf{r}_p) = |h_1(\mathbf{r}_p + \mathbb{M}_1(\mathbf{r}_o + \mathbf{r}_s)|^2 |h_2((\mathbf{r}_o + \mathbf{r}_s) + \mathbb{M}_2 \mathbf{r}_d)|^2 \tag{60}$$

and

$$H_{\text{cv}}(\mathbf{r}_s, \mathbf{r}_o, \mathbf{r}_p) = |h_1(\mathbf{r}_p + \mathbb{M}_1(\mathbf{r}_o + \mathbf{r}_s)|^2 \tag{61}$$

respectively. Comparing equations (60) and (61) to equations (53) and (54) it is seen that the intensity PSFs for the coherent and incoherent systems are identical in form. That said the resulting images differ by virtue of the difference between equations (39) and (58).

As highlighted by Gu in [23], the equivalence of the intensity PSFs in coherent and incoherent imaging systems highlights the inadequacy of the PSF description of imaging systems. Instead an OTF description is deemed more fundamental since differences can be seen here.

Indeed, following [35], the 3D OTF in an incoherent system is defined as the 3D inverse Fourier transform of the intensity PSF *viz.*

$$\widetilde{H}(\mathbf{m}) = \int H(\mathbf{r}_1) \exp[-2\pi i \mathbf{r}_1 \cdot \mathbf{m}] d^3\mathbf{r}_1. \tag{62}$$

Defining the object and image spectrum in a similar fashion as

$$\widetilde{T}(\mathbf{m}) = \int T(\mathbf{r}_1) \exp[-2\pi i \mathbf{r}_1 \cdot \mathbf{m}] d^3\mathbf{r}_1 \tag{63}$$

and

$$\widetilde{I}(\mathbf{m}) = \int I_d(\mathbf{r}_s, \mathbf{r}_p) \exp[-2\pi i \mathbf{r}_s \cdot \mathbf{m}] d^3\mathbf{r}_s \tag{64}$$

the convolution integral expressed in equation (58) can be written in the Fourier domain as

$$\widetilde{I}(\mathbf{m}) = \widetilde{H}(\mathbf{m})\widetilde{T}(\mathbf{m}). \tag{65}$$

In relation to the definition of the OTF given in equation (62) it is important to note that whilst for the confocal case the intensity PSF is given by the square of the amplitude PSF, the OTF is not given by the square of the CTF. The incoherent OTF is in fact related to the CTF of the analogous system *via* a convolution integral *viz.*

$$\widetilde{H}_{\text{cf}}(\mathbf{m}) = \widetilde{H}_{\text{cf}-1}(\mathbf{m}) \otimes_3 \widetilde{H}_{\text{cf}-2}(\mathbf{m}) \tag{66}$$

where

$$\widetilde{H}_{\text{cf}-n}(\mathbf{m}) = \int |h_n(\mathbf{r})|^2 \exp[-2\pi i \mathbf{r} \cdot \mathbf{m}] d^3\mathbf{r} \tag{67}$$

$$= \int \widetilde{h}_n^*(\mathbf{m}' - \mathbf{m})\widetilde{h}_n(\mathbf{m}') d^3\mathbf{m}' = \widetilde{h}_n^*(\mathbf{m}) \star \widetilde{h}_n(\mathbf{m}'), \tag{68}$$

$\star$ denotes a 3D correlation and

$$\widetilde{h}_n^*(\mathbf{m}) = \int h_n(\mathbf{r}) \exp[-2\pi i \mathbf{r} \cdot \mathbf{m}] d^3\mathbf{m}. \tag{69}$$

Likewise for a conventional imaging arrangement the incoherent OTF is given by the auto-correlation of the amplitude PSF of the objective lens *i.e.* $\widetilde{H}_{\text{cv}}(\mathbf{m}) = \widetilde{h}_1^*(\mathbf{m}) \star \widetilde{h}_1(\mathbf{m})$. This observation will be required in Section 3.

2.4 Confocal and conventional interferometeric setups

Interferometric microscopes can be found in numerous configurations, such as the Linnik, Mirau, Michelson, Fizeau, Mach-Zender or confocal interferometers [51]. Each has their own advantages and disadvantages [52], however, in all geometries the field scattered from the object is combined with that of a reference beam. Imaging in an interference microscope has previously been considered in, for example, [40, 53, 54, 55]. The setup considered in [40], for example, is based upon a Mach-Zender configuration. Moreover it should be noted that a digital holographic microscope (DHM) is based upon a Mach-Zender architecture, albeit without any lenses present in the reference arm [34]. As such the wavefront in the reference arm is less important in a DHM [56, 57]. Derivations for the CTF of a confocal interferometer and a fibre-optical confocal interferometer can be found in [58, 23].

In this section both confocal and conventional interferometric microscopy setups are considered and the associated CTF derived. Confocal interferometric microscopy, for example forms the basis of optical coherence systems (such as optical coherence tomography (OCT)), whilst a coherence probe microscope (CPM) is an example of a conventional interference microscope [59] commonly found in surface profilometry [60].

To derive the CTF for interferometric imaging it must first be noted that the intensity at a point $\mathbf{r}_2$ in detector space is given by

$$\begin{aligned} I_{\mathrm{i}}(\mathbf{r}_2) &= |E_d(\mathbf{r}_2)|^2 + |E_{\mathrm{ref}}(\mathbf{r}_2)|^2 + E_d(\mathbf{r}_2)E^*_{\mathrm{ref}}(\mathbf{r}_2) + E^*_d(\mathbf{r}_2)E_{\mathrm{ref}}(\mathbf{r}_2) && (70)\\ &= |E_d(\mathbf{r}_2)|^2 + |E_{\mathrm{ref}}(\mathbf{r}_2)|^2 + 2\Re\left[E_d(\mathbf{r}_2)E^*_{\mathrm{ref}}(\mathbf{r}_2)\right] && (71)\\ &= I_d(\mathbf{r}_2) + I_{\mathrm{ref}}(\mathbf{r}_2) + I_{\mathrm{int}}(\mathbf{r}_2) && (72)\end{aligned}$$

where $E_{\mathrm{ref}}(\mathbf{r}_2)$ is the reference field (and the dependence on $\mathbf{r}_p$ and $\mathbf{r}_s$ has been omitted for clarity). Three contributions can be identified namely two non-interference terms arising from the object and reference beam, plus a term from the interference of the object and reference field. For simplicity it will be assumed that in the reference arm the scattering function is given by a complex constant, r, as appropriate to reflection by a mirror, *i.e.* $t_{\mathrm{ref}}(\mathbf{r}_1) = r\delta(z_1)$. Note the associated spectrum is $\widetilde{t}_{\mathrm{ref}}(\mathbf{m}) = r\delta(m)\delta(n)$. For a general detection geometry the reference field intensity is given, in analogy to (40), by

$$\begin{aligned} I_{\mathrm{ref}}(\mathbf{r}_2, \mathbf{r}_p) &= \iint \widetilde{H}_{\mathrm{ref}}(\mathbf{m}, \mathbf{m}')\widetilde{t}_{\mathrm{ref}}(\mathbf{m})\widetilde{t}^*_{\mathrm{ref}}(\mathbf{m}')\, d^3\mathbf{m}\, d^3\mathbf{m}' && (73)\\ &= \iint \widetilde{H}_{\mathrm{ref}}(0, 0, q, 0, 0, q')dqdq'. && (74)\end{aligned}$$

It is noted that the reference object is not scanned such that $\mathbf{r}_s$ in equation (40) has been set to zero without loss of generality. Here, in analogy to (42),

$$\widetilde{H}_{\mathrm{ref}}(\mathbf{m}, \mathbf{m}') = \int \widetilde{h}_{\text{cf-ref}}(\mathbf{m}, \mathbf{r}_2, \mathbf{r}_p)\widetilde{h}^*_{\text{cf-ref}}(\mathbf{m}', \mathbf{r}_2, \mathbf{r}_p)D(\mathbf{r}_2)d^3\mathbf{r}_2 \tag{75}$$

and

$$\begin{aligned} \widetilde{h}_{\text{cf-ref}}(\mathbf{m}, \mathbf{r}_2, \mathbf{r}_p) = \int &\exp[ik(z_p - z_2 - 2z_1)]h_{\mathrm{ref}-1}(\mathbf{r}_p + \mathbb{M}_1\mathbf{r}_1)\\ &\times h_{\mathrm{ref}-2}(\mathbf{r}_1 + \mathbb{M}_2\mathbf{r}_2)\exp[-2\pi i\mathbf{r}_1 \cdot \mathbf{m}]d^3\mathbf{r}_1 \end{aligned} \tag{76}$$

where a difference in the pupil function of the reference arm lenses has been allowed for. Simplifications can follow, however, by noting

$$\widetilde{h}_{\text{cf-ref}}(\mathbf{m}, \mathbf{r}_2, \mathbf{r}_p) = \int \widetilde{h}_{\text{cf-ref}}(m, n, z_1, \mathbf{r}_2, \mathbf{r}_p) \exp[-2\pi i q z_1] dz_1 \tag{77}$$

such that

$$\begin{aligned}\widetilde{h}_{\text{cf-ref}}(0, 0, q, \mathbf{r}_p, \mathbf{r}_2) = e^{ik(z_p - z_2)} \iint & P_{\text{ref}-1}(\zeta, \eta) P_{\text{ref}-2}(-\zeta, -\eta) \delta\left(q + \frac{2}{\lambda}\right) \\ & \times \exp\left[\frac{ik}{d_1}(\zeta(x_p - x_2) + \eta(y_p - y_2))\right] \\ & \times \exp\left[-\frac{ik}{2d_1^2}(\zeta^2 + \eta^2)(z_p - z_2)\right] d\zeta d\eta. \end{aligned} \tag{78}$$

From equations (43) and (44) it is possible to show that the reference beam intensities are given by

$$\begin{aligned} I_{\text{cf-ref}}(\mathbf{r}_d, \mathbf{r}_p) = |r|^2 \Bigg| \iint & P_{\text{ref}-1}(\zeta, \eta) P_{\text{ref}-2}(-\zeta, -\eta) \\ & \times \exp\left[\frac{ik}{d_1}(\zeta(x_p - x_d) + \eta(y_p - y_d))\right] \\ & \times \exp\left[-\frac{ik}{2d_1^2}(\zeta^2 + \eta^2)(z_p - z_d)\right] d\zeta d\eta \Bigg|^2 \end{aligned} \tag{79}$$

and

$$I_{\text{cv-ref}}(\mathbf{r}_p) = |r|^2 \iint |P_{\text{ref}-1}(\zeta, \eta)|^2 \, |P_{\text{ref}-2}(-\zeta, -\eta)|^2 \, d\zeta d\eta. \tag{80}$$

More interesting are the interference terms since these carry information about the object. The point-wise intensity in detector space is given by a term of the form

$$\begin{aligned} E_d(\mathbf{r}_2, \mathbf{r}_p) E^*_{\text{ref}}(\mathbf{r}_2, \mathbf{r}_p) = \iint & \widetilde{h}_{\text{cf}}(\mathbf{m}, \mathbf{r}_2, \mathbf{r}_p) \widetilde{h}^*_{\text{cf-ref}}(\mathbf{m}', \mathbf{r}_2, \mathbf{r}_p) \\ & \times \widetilde{t}(\mathbf{m}) \widetilde{t}^*_{\text{ref}}(\mathbf{m}') \exp[2\pi i \mathbf{r}_s \cdot \mathbf{m}] d^3\mathbf{m} d^3\mathbf{m}' \end{aligned} \tag{81}$$

$$\begin{aligned} = r^* \iint & \widetilde{h}_{\text{cf}}(\mathbf{m}, \mathbf{r}_2, \mathbf{r}_p) \widetilde{h}^*_{\text{cf-ref}}(0, 0, q', \mathbf{r}_2, \mathbf{r}_p) \\ & \times \widetilde{t}(\mathbf{m}) \exp[2\pi i \mathbf{r}_s \cdot \mathbf{m}] d^3\mathbf{m} dq'. \end{aligned} \tag{82}$$

The recorded intensity for each scan point is then given by

$$I_{\text{int}}(\mathbf{r}_s, \mathbf{r}_p) = \int 2\Re \left[E_d(\mathbf{r}_2) E^*_{\text{ref}}(\mathbf{r}_2) D(\mathbf{r}_2) d\mathbf{r}_2\right] \tag{83}$$

$$= 2\Re \left[\int \widetilde{h}_{\text{int}}(\mathbf{m}, \mathbf{r}_p) \widetilde{t}(\mathbf{m}) \exp[2\pi i \mathbf{r}_s \cdot \mathbf{m}] d^3\mathbf{m}\right] \tag{84}$$

where $\widetilde{h}_{\text{int}}(\mathbf{m},\mathbf{r}_p)$ is the interference CTF given by

$$\widetilde{h}_{\text{int}}(\mathbf{m},\mathbf{r}_p) = r^* \iint \widetilde{h}_{\text{cf}}(\mathbf{m},\mathbf{r}_2,\mathbf{r}_p)\widetilde{h}^*_{\text{cf-ref}}(0,0,q',\mathbf{r}_2,\mathbf{r}_p)D(\mathbf{r}_2)d^3\mathbf{r}_2 dq'. \tag{85}$$

By substituting in earlier expressions and performing the integrations explicitly where possible, it can be shown that for the confocal and conventional cases, the interference CTF is given by

$$\begin{aligned}
\widetilde{h}_{\text{cf-int}}(\mathbf{m},\mathbf{r}_p) = r^* \iiiint & P_1(\zeta,\eta)P_2(m\lambda d_2-\zeta, n\lambda d_2-\eta)P^*_{\text{ref}-1}(\zeta',\eta')P^*_{\text{ref}-2}(-\zeta',-\eta') \\
&\times \exp\left[\frac{ik}{d_1}(\zeta x_p+\eta y_p)\right]\exp\left[\frac{ik}{d_1}((m\lambda d_2-\zeta)x_d+(n\lambda d_2-\eta)y_d)\right] \\
&\times \exp\left[-\frac{ik}{2d_1^2}z_p(\zeta^2+\eta^2)\right]\exp\left[-\frac{ik}{d_1}(\zeta'(x_p-x_d)+\eta'(y_p-y_d))\right] \\
&\times \exp\left[\frac{ik}{2d_1^2}z_d((m\lambda d_2-\zeta)^2+(n\lambda d_2\eta)^2)\right]\exp\left[\frac{ik}{2d_1^2}(z_p-z_d)(\zeta'^2+\eta'^2)\right] \\
&\times \delta\left(q+\frac{2}{\lambda}+(m^2+n^2)\frac{\lambda}{2}-\frac{m\zeta}{d_2}-\frac{n\eta}{d_2}\right)d\zeta d\eta d\zeta' d\eta'
\end{aligned} \tag{86}$$

and

$$\begin{aligned}
\widetilde{h}_{\text{cv-int}}(\mathbf{m},\mathbf{r}_p) = r^* \iint & P_1(\zeta,\eta)P_2(m\lambda d_2-\zeta, n\lambda d_2-\eta) \\
&\times P^*_{\text{ref}-1}(m\lambda d_2-\zeta, n\lambda d_2-\eta)P^*_{\text{ref}-2}(-m\lambda d_2+\zeta,-n\lambda d_2+\eta) \\
&\times \exp\left[-\frac{ik}{2d_1^2}z_p(\zeta^2+\eta^2)\right]\exp\left[-\frac{ik}{d_1}((m\lambda d_2-2\eta)x_p+(n\lambda d_2-2\eta)y_p\right] \\
&\times \exp\left[\frac{ik}{2d_1^2}z_p((m\lambda d_2-\eta)^2+(n\lambda d_2-\eta)^2\right] \\
&\times \delta\left(q+\frac{2}{\lambda}+(m^2+n^2)\frac{\lambda}{2}-\frac{m\zeta}{d_2}-\frac{n\eta}{d_2}\right)d\zeta d\eta
\end{aligned} \tag{87}$$

respectively. Assuming the point source (and point detector for the confocal case) are located such that $\mathbf{r}_p = \mathbf{r}_d = 0$ these equations reduce to

$$\begin{aligned}
\widetilde{h}_{\text{cf-int}}(\mathbf{m},\mathbf{0}) = r^* \iiiint & P_1(\zeta,\eta)P_2(m\lambda d_2-\zeta, n\lambda d_2-\eta)P^*_{\text{ref}-1}(\zeta',\eta')P^*_{\text{ref}-2}(-\zeta',-\eta') \\
&\times \delta\left(q+\frac{2}{\lambda}+(m^2+n^2)\frac{\lambda}{2}-\frac{m\zeta}{d_2}-\frac{n\eta}{d_2}\right)d\zeta d\eta d\zeta' d\eta'
\end{aligned} \tag{88}$$

and

$$\begin{aligned}
\widetilde{h}_{\text{cv-int}}(\mathbf{m},\mathbf{0}) = r^* \iint & P_1(\zeta,\eta)P_2(m\lambda d_2-\zeta, n\lambda d_2-\eta) \\
&\times P^*_{\text{ref}-1}(m\lambda d_2-\zeta, n\lambda d_2-\eta)P^*_{\text{ref}-2}(-m\lambda d_2+\zeta,-n\lambda d_2+\eta) \\
&\times \delta\left(q+\frac{2}{\lambda}+(m^2+n^2)\frac{\lambda}{2}-\frac{m\zeta}{d_2}-\frac{n\eta}{d_2}\right)d\zeta d\eta.
\end{aligned} \tag{89}$$

2.5 Monochromatic vs. polychromatic illumination

Thus far consideration has been restricted to a monochromatic treatment, however, numerous polychromatic metrology techniques exist, such as optical coherence tomography (OCT), coherence scanning interferometry (CSI), confocal chromatic microscopy (CCM) and dispersive scanning interferometry (DSI) [2]. Implicit in the earlier results is a dependence on the illumination wave, *via* $k = 2\pi/\lambda$. It is possible to define a polychromatic transfer function by integrating the monochromatic transfer function [61, 62, 63, 64, 65, 66], however, this approach is only valid under the assumption that the object function $t(\mathbf{r})$ is itself not dependent on the wavelength. Given the usual definition of the scattering potential in Section 2.1, it is evident that this does not hold, due to a dependence on both illumination wavenumber k and refractive index. The k^2 factor in the scattering potential can however be absorbed into the appropriate expressions for the transfer function (see *e.g.* [67]). Such an approach will naturally accomodate chromatic aberrations and dispersive effects of the measurement system. Dispersive effects of the sample may, however, exist as will be parameterised within the refractive index term of the scattering potential. Assuming, however, that no strong material resonances exist within the illumination bandwidth, these effects will be weak. These conditions are assumed to apply here, so that a polychromatic CTF may be defined as

$$\widetilde{h}_{\text{poly}}(\mathbf{m}, \mathbf{r}_2, \mathbf{r}_p,) = \int \widetilde{h}_{\text{mono}}(\mathbf{m}, \mathbf{r}_2, \mathbf{r}_p, \lambda) s(\lambda) d\lambda \tag{90}$$

where $s(\lambda)$ represents the (complex) amplitude of each spectral component. Accordingly the polychromatic TCC follows as

$$\widetilde{H}_{\text{poly}}(\mathbf{m}, \mathbf{m}') = \iiint \widetilde{h}_{\text{mono}}(\mathbf{m}, \mathbf{r}_2, \mathbf{r}_p, \lambda) \widetilde{h}^*_{\text{mono}}(\mathbf{m}', \mathbf{r}_2, \mathbf{r}_p, \lambda') \langle s(\lambda) s^*(\lambda') \rangle d\lambda d\lambda' d^3\mathbf{r}_2 \tag{91}$$

where the angular brackets $\langle \cdot \rangle$ denote the temporal average. If strong phase coherence is present between spectral components then $\langle s(\lambda) s^*(\lambda') \rangle = s(\lambda) s^*(\lambda')$. Conversely for a temporally incoherent source, such as an incandescent lamp $\langle s(\lambda) s^*(\lambda') \rangle = s(\lambda) s^*(\lambda') \delta(\lambda - \lambda') = S(\lambda) \delta(\lambda - \lambda')$ such that

$$\widetilde{H}_{\text{poly}}(\mathbf{m}, \mathbf{m}') = \iint R(\lambda) \widetilde{h}_{\text{mono}}(\mathbf{m}, \mathbf{r}_2, \mathbf{r}_p, \lambda) \widetilde{h}^*_{\text{mono}}(\mathbf{m}', \mathbf{r}_2, \mathbf{r}_p, \lambda) S(\lambda) D(\mathbf{r}_2) d\lambda d^3\mathbf{r}_2 \tag{92}$$

$$= \int R(\lambda) \widetilde{H}_{\text{mono}}(\mathbf{m}, \mathbf{m}', \lambda) S(\lambda) d\lambda \tag{93}$$

where the spectral response $R(\lambda)$ of the detector has also been introduced for completeness. Ultimately the image intensity is given once more by equation (42) with use of the polychromatic TCC instead of the monochromatic TCC. Care must however be taken in employing the polychromatic version of equation (42) due to the underlying assumption of shift invariance required in the definition of a transfer function. Particularly, whilst shift-invariance may hold for each spectral component individually, this in itself does not guarantee that the polychromatic image will be shift invariant. Considering the basic imaging equations it can be seen that polychromatic shift invariance will not hold if the magnification of the imaging system $\mathbb{M}_1$ or $\mathbb{M}_2$ is strongly wavelength dependent [62]. Further dangers of using polychromatic transfer functions, arising from the possibility of non-uniqueness, have been highlighted in [68].

2.6 High numerical aperture systems

The discussion presented thus far has been based upon low numerical aperture optics, such that a paraxial approximation could be made and the amplitude point spread function of a lens could be written as the Fourier transform of the pupil function as per equation (19). For high NA (*i.e.* NA $\gtrsim 0.5$) systems however departures from this theory arise due to three main effects. The first of these is that waves propagating in the system can do so at large angles to the optical axis, such that the paraxial approximation is no longer valid. Secondly, polarisation properties of light become important due to the introduction of a non-negligible longitudinal component in object space. Finally an apodisation across the pupil also occurs.

Sheppard *et al.* [69, 70] have approached the generalisation of the OTF to high NA functions avoiding the paraxial approximation, however vectorial effects were not included. The apodisation effect has also be considered [71]. In moving away from a low NA system the pupil function of a lens can no longer be specified in the pupil plane of the lens. Instead, the pupil function must be specified over the surface of the Gaussian reference sphere located in the exit pupil centered on the geometric focus of the lens. The 3D CTF of a single lens can therefore be shown to be given by [29]

$$\widetilde{h}(\mathbf{m}) = \frac{P(m,n)}{\sqrt{1-q^2}}\,\delta\left(q+\sqrt{1-m^2-n^2}\right). \tag{94}$$

Whilst this expression can be used in earlier equations, such as equation (27), it should be noted that subsequent analytic integrations can frequently not be performed.

Vectorial transfer functions have furthermore be considered within a paraxial regime by Urbańczyk [72, 73, 74], albeit this work considered only 2D image formation. A fuller 3D vectorial theory has however been proposed by Arnison and Sheppard [75] and Sheppard and Larkin [76] which also relaxes the paraxial approximation. Polarisation properties will not be considered any further here however, due to the extra level of complexity required to fully account for such features and the additional difficulties associated with measuring such a transfer function. Measurements of such vectorial transfer function are also difficult to find in the literature.

A final issue worthy of note is the assumption of shift invariance in high NA imaging systems. Particularly the amplitude PSF is, in general, not shift invariant such that this assumption is not valid. If however 3D object scanning is used it is evident that the imaging properties of the optical system are unchanged with object position, such that 3D shift invariance can safely be assumed. Full 3D object scanning is however not required if the lens satisfies the sine condition, such that the apodisation function takes the form $a(\theta) = \sqrt{\cos\theta}$, which produces transverse shift invariance. Full 3D shift invariance can hence be maintained if only axial object scanning is used. Conversely, if the lens satisfies the Herschel condition, axial shift invariance follows, however this necessitates transverse object scanning to maintain full 3D shift invariance [29].

2.7 Surface topography measurements

Whilst surface topography measurements represent a class of 3D imaging measurements in a broad sense, and are hence describable (under the correct conditions) by the framework given thus far, they are a special class. Accordingly further results may be expected to follow within this field of study. This is indeed true, as can be seen upon a reexamination of scattering from surfaces as is presented here.

Fundamentally when a surface is illuminated by a single plane wave, a spectrum of output plane waves can result. Surface scattering is therefore commonly formulated using a scattering function $\widetilde{S}(\mathbf{m}_1;\mathbf{m}_2)$ which describes the relative amplitude and phase between an input plane wave propagating in a direction defined by the direction cosines $\mathbf{m}_1 = (m_1, n_1, q_1)$ and one of the output plane waves propagating in a direction defined by the direction cosines $\mathbf{m}_2 = (m_2, n_2, q_2)$ [77] (see Figure 2). If however the radius of curvature at each point on the surface can be considered to be much greater than the wavelength, the surface can be considered to be locally plane, such a single input plane wave gives rise to a single output plane wave dependent on the tilt of the surface. Under these circumstances it is logical to change coordinate systems to $\mathbf{m} = \mathbf{m}_1 - \mathbf{m}_2$, where it is also noted that $\mathbf{m}$ represents the spatial frequency components of the surface. This is known as the Kirchoff approximation [78]. Under this approximation the scattering function can be written in the form $\widetilde{S}(\mathbf{m})$. Such a replacement is also possible if the surface height variations are small [77]. The image amplitude following scattering from the surface can then be written in the form

$$E_d(\mathbf{r}_s, \mathbf{r}_s, \mathbf{r}_p) = \int \widetilde{h}_{\mathrm{cf}}(\mathbf{m}, \mathbf{r}_2, \mathbf{r}_p)\widetilde{S}(\mathbf{m}) \exp[2\pi i \mathbf{r}_s \cdot \mathbf{m}] d^3\mathbf{m} \tag{95}$$

which should be compared with equation (30).

Provided that the surface is smooth at the optical scale and there is negligible multiple scattering, the 3D object can indeed be replaced by an infinitely thin "foil" like object placed at the interface. Indeed, using this model, it has been shown that for a 1D perfectly conducting surface, illuminated by s-polarised light, the scattering function can be written in the form [78]

$$\widetilde{S}(m, q) = \left(\frac{m^2 + q^2}{2q}\right) \int \exp\left[-2\pi i(mx + qZ(x))\right] dx. \tag{96}$$

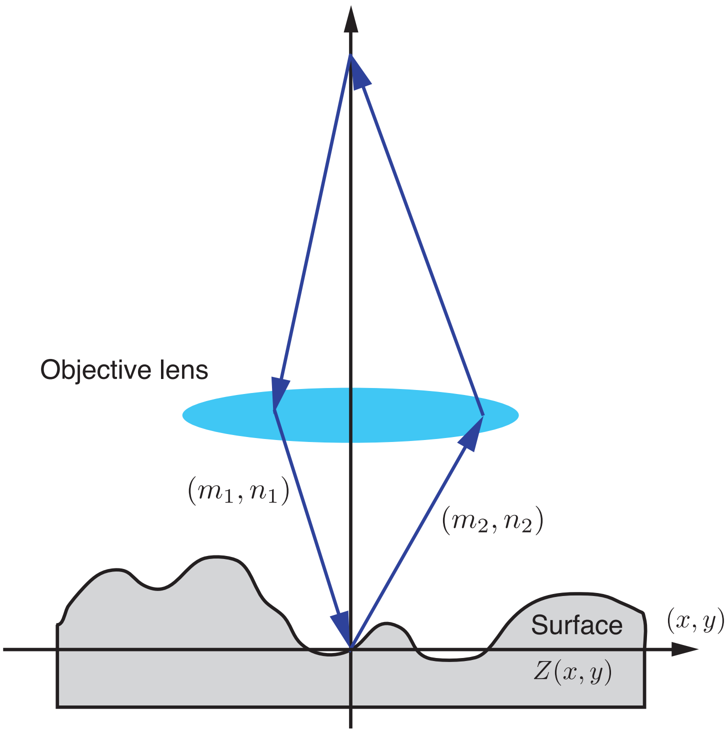

Figure 2: Simplified geometry of surface measurement depicting an incident plane wave with direction defined by (m_1, n_1) scattered to a plane wave with direction (m_2, n_2).

This result was later extended to 2D surfaces [77] and reads

$$\widetilde{S}(\mathbf{m}) = \left(\frac{m^2+n^2+q^2}{2q}\right) \iint \exp\left[-2\pi i(mx+ny+sZ(x))\right] dx \tag{97}$$

$$= \left(\frac{m^2+n^2+q^2}{2q}\right) \iint \delta(z - Z(x,y)) \exp\left[-ik(mx+ny+sz)\right] dx \tag{98}$$

$$= \left(\frac{m^2+n^2+q^2}{2q}\right) \widetilde{t}(\mathbf{m}) \tag{99}$$

where from Eqs. (98) and (99), $\widetilde{t}(\mathbf{m})$ is the 3D Fourier transform of the surface profile, *i.e.* the object spectrum as before. The geometric pre-factor introduced when considering surface scattering reduces to unity for low numerical aperture systems. Equations (30), (95) and (99) show that for surface measurements the effective CTF becomes

$$\widetilde{h}_{\text{cf-sur}}(\mathbf{m}) = \left(\frac{m^2+n^2+q^2}{2q}\right) \widetilde{h}_{\text{cf}}(\mathbf{m}). \tag{100}$$

Earlier expressions derived for coherent, incoherent, partially coherent and interferometric imaging systems are all dependent on the CTF $\widetilde{h}_{\text{cf}}(\mathbf{m})$ when imaging 3D objects. Given equation (100) these results are still applicable with the replacement $\widetilde{h}_{\text{cf}}(\mathbf{m}) \rightarrow \widetilde{h}_{\text{cf-sur}}(\mathbf{m})$ in the appropriate formulae.

3 Measurement of 3D transfer functions

The first part of this report has focused on laying out the theory of transfer functions in optical imaging systems. Formulations of this nature were pursued with a view to calibration of metrology systems. It has long been recognised that such calibration and characterisation of measurement systems can be obtained by measurement of either the 3D PSF or the associated transfer function [79, 80]. This has become increasingly sought as measurement protocols have moved away from more traditional parameters, such as surface roughness or form, towards measuring the full power spectral density of a 3D object or surface [81, 82, 83, 84]. Accordingly the latter portion of this report turns attention to the measurement of the transfer function of optical imaging and interferometric setups. Due to the relationships expounded above between the 3D PSF and the 3D transfer function, direct measurement of the PSF can also be considered as a measurement of the transfer function in some (but not all) cases.

Given the assortment of imaging setups possible, distinction must be made as to which transfer function is to be measured. For example, if a confocal reflection microscope is used for surface profiling [85] calibration requires measurement of the complex CTF, whilst for a confocal interferometric setup the interference CTF must instead be measured [58]. Alternatively, in a spatially incoherent system, the OTF is required. Different measurement procedures must hence be pursued in each case and care taken in selecting the appropriate acquisition and processing technique.

To highlight this issue consider first the possible forms of the imaging equations, expressed in terms of the relevant transfer function, which are stated here for clarity. Specifically for a spatially fully, partially and in- coherent setup the imaging equations are

$$I_{\text{coh}}(\mathbf{r}_s) = \left| \int \widetilde{h}(\mathbf{m})\widetilde{t}(\mathbf{m}) \exp[2\pi i \mathbf{r}_s \cdot \mathbf{m}] d\mathbf{m} \right|^2 \tag{101}$$

$$I_{\text{pc}}(\mathbf{r}_s) = \iint \widetilde{H}(\mathbf{m}, \mathbf{m}')\widetilde{t}(\mathbf{m})\widetilde{t}^*(\mathbf{m}') \exp[2\pi i \mathbf{r}_s \cdot (\mathbf{m} - \mathbf{m}')]\, d^3\mathbf{m}\, d^3\mathbf{m}' \tag{102}$$

$$I_{\text{inc}}(\mathbf{r}_s) = \int \widetilde{H}(\mathbf{m})\widetilde{T}(\mathbf{m}) \exp[2\pi i \mathbf{r}_s \cdot \mathbf{m}] d^3\mathbf{m} \tag{103}$$

respectively where the separability of the TCC in the coherent case has been emphasised. Henceforth it is also assumed that $\mathbf{r}_p = \mathbf{0}$ for simplicity and hence the functional dependence dropped. Supplementing these equations with that of an interferometric setup, *i.e.*,

$$I_{\text{int}}(\mathbf{r}_s) = 2\Re \left[\int \widetilde{h}(\mathbf{m})\widetilde{t}(\mathbf{m}) \exp[2\pi i \mathbf{r}_s \cdot \mathbf{m}] d^3\mathbf{m} \right] \tag{104}$$

yields the complete set of equations to be considered here (equations (101)-(104)). Following the discussion in Section 2.5 it is noted that the transfer functions of equations (101)-(104) may be either monochromatic or polychromatic as appropriate for the system under study. Before existing literature on measurement of the transfer function is reviewed, it is important to mention that many such works aim to measure only a 2D transfer function. Given equation (33) (and its analog for the other system geometries under consideration) it is evident that all such techniques can be employed for measurement of the 2D defocused transfer function, by introducing a variable defocus of the test object into the system, such that a 3D image stack can be acquired to ultimately allow reconstruction of the full 3D transfer function. Measurements of 2D transfer functions will hence also be included within the following review.

3.1 Incoherent systems

Solution of the imaging equations for the transfer function is simplest for an incoherent system such that equation (103), or equivalently equation (65), holds. Solution for the OTF then quickly follows by taking the ratio of a measured image spectrum obtained from a known object with the spectrum of the object distribution, *i.e.*

$$\widetilde{H}(\mathbf{m}) = \widetilde{I}(\mathbf{m})/\widetilde{T}(\mathbf{m}). \tag{105}$$

The majority of techniques to experimentally measure the OTF were developed during the 1940's to the 1960's [80, 86], many based on this approach. Knowledge of the form of the sample object is however crucial to accurate determination of the OTF. Moreover, judicious choice of the sample object must be made so as to avoid zeros in its spectrum, in turn implying the transfer function can not be determined over a complete range of frequencies. Historically a plethora of alternative structures and standard targets have indeed been employed in the measurement of the OTF each with their own merits. Many works, however, only aim to measure the MTF. Whilst the MTF by itself does not contain complete information about the optical system, it is often sought if only a parameter derived from the full image data, such as surface height, is available instead of the image data itself [87], as may be true for commercial systems. In this case it is more appropriate to say that it is the instrument transfer response function which is sought, however there is no guarantee that intermediate processing steps include solely linear operations as required for a transfer function description to be valid. Alternatively an implicit assumption that the PSF is symmetric (and hence an even function) is made, in turn yielding a purely real OTF. This latter assumption must, however, be viewed with caution since it will not hold in general, especially for an aberrated system.

Equation (62) encapsulates perhaps the most intuitive method by which to measure the OTF in an incoherent system. In particular if a point object is used as a test object, the acquired image can be directly Fourier transformed to give the complete complex OTF, from which the MTF and PTF can easily be found. Equivalently this can be seen from equation (105) since the 3D spectrum of an ideal point object (mathematically represented by a Dirac delta function) is a uniform, isotropic distribution, *i.e.* $\widetilde{T}(\mathbf{m}) = 1$ for all $\mathbf{m}$. True sources, however, possess a finite size in turn introducing a frequency dependence in the object spectrum (albeit a weak dependence). If however $r_0 \ll \lambda/4$ the object spectrum is approximately uniform such that the source can be considered effectively as a point. Measurement of the PSF has indeed received much attention, particularly due to the availability of individual fluorophores, such as fluorescent dyes or quantum dots, that represent effective point sources due to their size. 3D measurements of the intensity PSF have hence been made by authors such as Agard *et al.* [88], Gibson and Lanni [89], and Goodwin [90]. Hiraoka *et al.* similarly collect a series of 2D defocused images of the intensity PSF from which they proceed to calculate the OTF [91]. Protocols have further been developed to measure the intensity PSF of a confocal fluorescence microscope [92]. Measurements obtained using CCDs are however limited by pixel size, as such Rhodes *et al.* measure the intensity PSF of a lens directly using a near field probe [93]. Given that a point source is inherently spatially coherent any measured amplitude PSF determined *via* coherent detection (see Section 3.2) can be used to find the intensity PSF (by taking the modulus and squaring c.f. equations (60) and (61)) appropriate to use of the imaging setup in an incoherent modality. In this vein, Beverage *et al.* use a Shack-Hartmann sensor to measure the complex wavefront in the exit pupil of a 3D microscope [94]. The associated intensity PSF is then given by the modulus squared of the Fourier transform of the measured field distribution.

PSF measurements, however, can suffer significantly from low signal to noise ratios. Today rapid data acquisition allows multiple measurements to be obtained and averaged, hence improving signal to noise ratios. Furthermore highly sensitive detectors exist which can help mitigate this issue to some extent, however the use of a line object or knife edge inherently increases the energy transmitted, and hence the signal to noise ratio, by an order of magnitude [95]. The image of a line object is known as the line spread function (LSF), whilst that of an edge is the edge spread function (ESF), with the former given by the derivative of the latter [96, 97, 98]. In one dimension the OTF is given by the 1D inverse Fourier transform of the LSF, a fact exploited by many authors [99, 100, 101]. However, to obtain a 2D coverage of frequency space it becomes necessary to rotate the object, so as to introduce an azimuthal dependence [100]. Algorithms for direct determination of the OTF from the ESF have been explored in [96, 102] and are preferable over a line object based method, since the latter suffers from the finite width of the object, in a similar fashion to that discussed for a finite sized point source above. It should be noted that modern targets, such as the ISO 12233 target, still include knife-edge type objects to allow OTF measurements *via* this method. A comparison of OTF measurements using the edge technique and interferometric methods is presented in [103], wherein it is concluded that they perform comparably, albeit the edge method can be less accurate at low frequencies. Whilst the techniques listed above measure the 2D OTF, step like or spherical objects, being inherently 3D in nature, allow for more direct measurement of the 3D OTF [104, 86, 105] .

Given the physical meaning of the OTF a further intuitive choice of test object is that of a 3D sinusoidal grating. Since the spectrum of such an object ideally constitutes a single spatial frequency, equation (105) implies that the image spectrum directly yields the appropriate element of the OTF. In the context of sine wave targets it is common to find studies in which only the MTF is measured. Specifically, instead of calculating the Fourier transforms implied in equation (105), the MTF is directly calculated by taking the ratio of the modulation (or contrast), defined as

$$M = \frac{I_{\text{max}} - I_{\text{min}}}{I_{\text{max}} + I_{\text{min}}}, \tag{106}$$

where I_{max} and I_{min} are the maximum and minimum intensities, in the final image and that in the object distribution *i.e.* $\text{MTF} = M_{\text{img}}/M_{\text{obj}}$. Such a technique however is limited since only a single spatial frequency can be probed for a single target. Targets were hence quickly developed in which the spatial frequency of the pattern varied spatially across the extent of the object. The original sine wave tests of Selwyn [22] have already been mentioned, however this strategy was also pursued by other authors [106, 107], and still forms the basis of existing methods for more complicated systems [108, 109]. Fabrication of accurate sine wave gratings can however pose technical problems. Whilst in more recent years this has been overcome, for example by using the interference pattern formed from two (or more) plane waves to form a suitable grating [109] or modern lithographic procedures, originally the idea developed to employ square wave [95, 110], or even triangular [111] test patterns due to the relative ease with which they could be made. It should also be noted that such targets cover more of the spatial frequency domain in a single image. More modern targets include the Siemens star target [112], Ronchi rulings and the USAF 1951 resolution target [113] (see Figure 3).

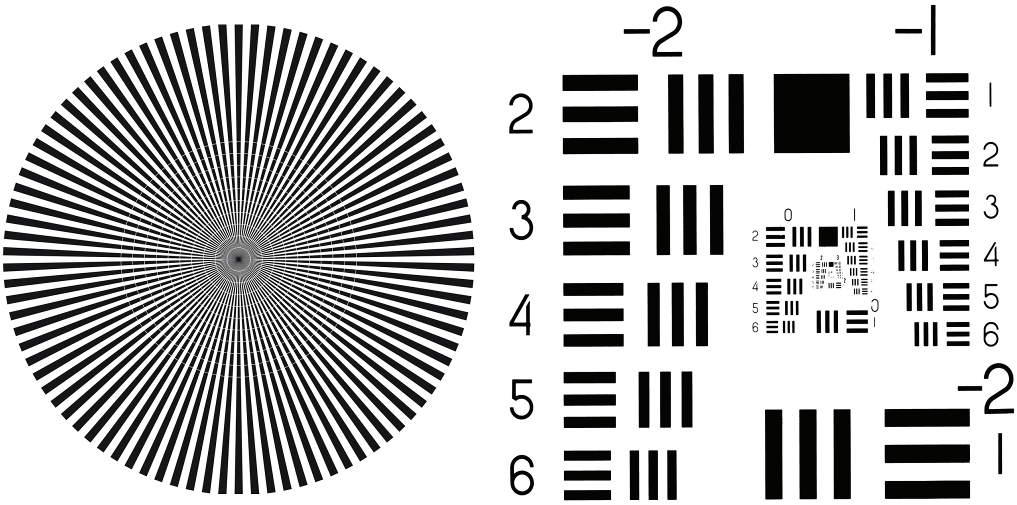

Figure 3: (left) Siemens star target and (right) USAF 1951 resolution target

A further class of 3D test object has been proposed, namely that of (pseudo-)random gratings [114], which has seen little attention until more recently [115, 116, 117]. Such a choice is motivated by the uniform power spectrum possessed by a pseudo-random grating.

Furthermore such gratings can be generated so as to possess shift-invariance, a property which has been shown to be locally violated in systems in which the image is sampled [118, 119, 120]. This technique furthermore improves the accuracy over those based on LSF/ESF measurements since high accuracy in these can only be achieved by using very narrow slits, which compromises signal levels [114]. The work detailed in [121, 87, 122, 123, 124, 121, 125, 126] similarly uses pseudo-random gratings (made *via* a standard lithographic process) as a test object, but here it is the MTF of the entire system, including effects from signal processing, detector response and environmental factors (as opposed to just the image forming optics), that is being measured. Polychromatic measurements of the MTF have also been made in [127, 128] by considering finite spectral bands, from which the polychromatic transfer function is subsequently calculated or directly measured [129, 130].

3.2 Coherent systems

Coherent systems (described by equation (101)) can be calibrated by measurement of their CTF. Many parallels can be drawn between measurement of the CTF in a coherent system and of an OTF in incoherent systems, albeit the discussion must proceed in terms of complex field amplitude instead of intensity, such that

$$\widetilde{h}(\mathbf{m}) = \widetilde{E}_d(\mathbf{m})/\widetilde{t}(\mathbf{m}), \tag{107}$$

where $\widetilde{E}_d(\mathbf{m})$ is the spectrum of the detected complex field amplitude. Accordingly an additional layer of difficulty is introduced since complete measurements of the field must measure both field amplitude and phase. Whilst the former can be found by taking the square root of an intensity image, the latter requires use of, say, a wavefront sensor or interferometer.

Following the structure of Section 3.1, consideration is first given to measurement of the amplitude PSF. To maintain phase coherence between the illumination beam and the collected scattered field, fluorescent sources can no longer be used for such a measurement. A number of solutions have been proposed in this vein, with Schrader *et al.*, for example, using 80 nm diameter colloidal gold particles immersed in immersion oil [131] (although phase was not measured by the authors). Cotte *et al.* use a 75 nm diameter nano-hole created *via* focused ion beam milling [132]. As with the measurements of the intensity PSF, the finite size of these sources will play a role in accurate determination of the OTF.

By far the most common method to measure the complex field amplitude is *via* interferometry as was first proposed within the context of OTF measurements by Hopkins [133] (albeit within a partially coherent context). Selligson [134] and Dandliker *et al.* [135] have used a Mach-Zender interferometer to measure the aberrations present in a lens by mapping the phase and intensity PSFs in the focal region of a lens. Similarly Schrader and Hell [136], and Török and Kao [137] used Tywman-Green interferormeters, whilst Juškaitis and Wilson [138] and Walford *et al.* [139] employed a fibre optic interferometer. Holographic measurements have also recently been reported [140, 132].

Despite the prevalence of interferometric methods, non-interferometric methods have been used for PSF measurements. For example, Beverage *et al.* have used a Shack-Hartmann sensor placed at the exit pupil of a microscope [94] from which the PSF can be found by a Fourier transform. Intensity only measurements can also be used if a phase retrieval algorithm is exploited [141, 142]. In this scenario complexity of the optical setup, is traded for additional noise amplification arising from the increased post-acquisition data processing.

Due to the difficulties of coherent detection in optical setups, such measurements are not common in the literature. That said both experimental and theoretical developments are well established in acoustic imaging in which the image formation process is analogous to that of optical systems [143, 144]. Within this domain both line and step functions have been used to determine the CTF of the imaging system [143, 145]. A theoretical study of spherical objects in a scanning confocal reflection acoustic microscope has been presented in [146, 147] whilst experimental measurements of the 2D defocused CTF are discussed in [148, 145, 149]. In these studies it was shown that a non-planar scan along the surface of a large steel sphere gives the in-focus CTF, whilst with small shifts of the focal position similar arc-scans give the 2D defocused CTF. Accordingly by forming 3D images near the top of the sphere the 3D CTF can be found. If considering measurement of the PTF only, then phase steps have also been shown to be suitable [150] for such measurements.

3.3 Partially coherent systems

Given that in partially coherent systems transmission of spatial frequencies must be described pairwise *via* a TCC (see equation (102)), measurement of such transmission characteristics becomes more involved. An approach based on division in the spatial frequency domain, as was adopted for coherent and incoherent systems alike, can no longer be pursued, since calculating the image spectrum *via* a Fourier transform yields only equal frequency values of the TCC i.e $\widetilde{H}(\mathbf{m}, \mathbf{m})$. For a conventional system it was shown earlier that the TCC is given by the autocorrelation of the pupil function (see equation (50)). Measurement of such an autocorrelation integral can be performed by inspection of the interference patterns arising from two identical but mutually shifted versions of the field. The lateral shift is commonly referred to as a shear of the field, such that the measurement setup is known as a shearing interferometer. Such an interferometer for determination of the autocorrelation of a field for OTF measurements was suggested by Hopkins [133] and first implemented in a Michelson-type geometry by Baker [151]. Variants of lateral shearing interferometers of this nature have since been proposed [152, 153, 154, 155, 156, 157, 158]. Setups in which rotating glass plates [159], double gratings [160, 161] and correlated partial diffusers [162] introduce the necessary shear between fields have also been developed. A scanning setup has also been proposed in [163].

3.4 Interferometric systems

As with partially coherent systems, measurement of the transfer function in interferometric systems requires a little more thought. Inspection of equation (104) highlights that once more a simple Fourier analysis does not directly yield the transfer function. The reason for this complication is that both the transfer function $\widetilde{h}(\mathbf{m})$ and object spectrum $\widetilde{t}(\mathbf{m})$ can be complex. For the object spectrum this will particularly be the case if the object exhibits any absorption, as is particularly the case with metallic materials. Any phase aberrations present in either the reference or object arm of the interferometer will likewise give rise to imaginary parts of the PSF and hence the transfer function.

Many commercial interferometer setups furthermore include a ground glass diffuser so as to reduce coherent noise, specifically speckle, that can arise from stray reflections and scattering in the optics. Specifically the interference pattern is imaged onto a rotating diffuser, which is subsequently relayed by a zoom lens onto a detector. In this way the interference image acts as an incoherent source for the relay optics, adding an additional step in the image formation process described by equation (103). This step shall, however, be neglected here for simplicity.

To establish how the transfer function of an interferometric imaging system can be determined it is first observed that equation (104) can be rewritten in the form

$$I_{\text{int}}(\mathbf{r}_s) = 2\int \left|\widetilde{h}(\mathbf{m}')\right| \left|\widetilde{t}(\mathbf{m}')\right| \cos[2\pi\mathbf{r}_s\cdot\mathbf{m}' + \Phi_h(\mathbf{m}') + \Phi_t(\mathbf{m}')] d^3\mathbf{m}' \tag{108}$$

where $\Phi_h(\mathbf{m})$ and $\Phi_t(\mathbf{m})$ are the phases of the transfer function and object spectrum respectively. Taking the Fourier transform yields

$$\begin{aligned}\widetilde{I}_{\text{int}}(\mathbf{m}) &= \int \left|\widetilde{h}(\mathbf{m}')\right| \left|\widetilde{t}(\mathbf{m}')\right| \big\{\exp[i\Phi_h(\mathbf{m}') + i\Phi_t(\mathbf{m}')]\delta(\mathbf{m}'-\mathbf{m})] \\ &\qquad + \exp[i\Phi_h(\mathbf{m}') + i\Phi_t(\mathbf{m}')]\delta(\mathbf{m}'+\mathbf{m})\big\}\, d^3\mathbf{m}' \qquad (109) \\ &= \widetilde{h}(\mathbf{m})\widetilde{t}(\mathbf{m}) + \widetilde{h}^*(-\mathbf{m})\widetilde{t}^*(-\mathbf{m}) \qquad (110)\end{aligned}$$

Due to the spatial frequency cutoffs of the transfer function [164, 165], equation (110) describes two separated copies of the product $\widetilde{h}(\mathbf{m})\widetilde{t}(\mathbf{m})$ (and its conjugate) in frequency space, such that one can be filtered as part of post-processing. The filtered spectrum is thus of the form $\widetilde{I}_{\text{int-fil}}(\mathbf{m}) = \widetilde{h}(\mathbf{m})\widetilde{t}(\mathbf{m})$ such that the interference CTF is given by

$$\widetilde{h}(\mathbf{m}) = \widetilde{I}_{\text{int-fil}}(\mathbf{m})/\widetilde{t}(\mathbf{m}). \tag{111}$$

Indeed such an approach has been adopted in [166, 167] upon acquisition of the PSF of the system using a coherence scanning inteferometer. The MTF of an OCT system has also been reported in [168, 169] by use of nanoparticles. Grid patterns have also been used to establish the PTF of a phase-shifting interferometer [170]. Novak *et al.* have used both phase steps and sine wave structures for characterising a Fizeau inteferometer [109]. Yashchuk *et al.* have shown that their proposed technique of using random gratings can be extended to measuring the MTF of interferometric systems, such as a Fizeau interferometer [125, 126]. An OTF measurement scheme, based on a shearing interferometer, using a white light source has also been proposed in [160] and is hence also suitable for study of white light interferometers or other polychromatic techniques.

4 Discussion

Optical transfer function theory covers an extensive array of optical systems ranging from spatially coherent to incoherent systems, monochromatic to white light sources and interferometric setups, yet it is the broad applicability and simplicity of the underlying principles which account for its success and prominence in the literature and beyond. Theoretical developments in this vein date back to before the invention of the laser, perhaps justifying the greater extent to which experimental studies have centered on partially coherent or incoherent setups. As optical technology has progressed however, so too has transfer function theory, with analytic expressions now available for many idealised optical configurations. Natural progression to the description of fully 3D systems is also clearly evident in the literature. Many practical systems are however far from ideal, yet despite this experimental measurement of transfer functions has seen slower development, especially for 3D imaging arrangements. Arguably such reticence likely follows from the greater ease with which alternative performance metrics, such as resolution, can be determined, *e.g.* by means of resolution targets. For many applications system characterisation by such incomplete means has proved adequate, yet now with the movement towards formulation of optical metrological standards, full system knowledge is required hence motivating accurate measurement of OTFs. Existing methods of performing OTF measurements have been reviewed in the latter portions of this text, however the question as to which method is preferred remains open. Predominantly OTF measurements all follow the same principle, namely measure the 3D "image" of an object with an accurately known spectrum (*i.e.* shape), from which the image spectrum and consequently the transfer function can be computed.

The question of optimality is not a trivial question to answer, however the key principles of a good measurement are clearly identifiable. In particular a good measurement should :

1. provide information across the full transmission bandwidth of the optical setup,
2. be well-posed, *i.e.* contain no zeros in the object spectrum,
3. be repeatable and robust,
4. be simple to implement, so as to allow and promote easy uptake by industrial users,
5. require objects which can practically (and cheaply) be manufactured.

Given requirement 1, techniques which employ multiple targets, *e.g.* sine wave targets or line gratings can immediately be excluded since these constitute a discrete set of object frequencies and hence the full system bandwidth is not covered and information is consequently lost. Targets such as a Siemens stars are also not suitable, since these probe spatial frequencies in one direction only (in this case the azimuthal direction) with no regard to variations in the radial or axial direction. Care must hence be taken to ensure variations exist in all three dimensions of any test object. Requirement 2 also directly precludes a number of targets. For example a square pillar, if chosen too large, will have zero crossings in its 3D spectrum which lie within the spatial bandwidth of the measuring system. Other examples of objects with zero crossings might include grooves. Such zeros inherent imply that no information regarding the value of the transfer function at the associated frequency is contained within the experimental data and hence solution is ill-posed.

Robustness (requirement 3) can be expressed in terms of the susceptibility of a measurement of a transfer function to noise. The first step to minimise the degrading effects of noise is to maximise the signal to noise ratio, by maximising light throughput in the system. Point objects are undesirable for this reason (as well as the associated difficulty in their manufacture). Assuming experimental conditions are maintained (*i.e.* noise levels upon detection are constant) it is the post processing of the raw image stack which will dominate overall noise properties on the inferred transfer function. Consider, for example, determining the OTF or CTF via equations (105) or (107) in which the experimental image is divided by the known object spectrum (an intuitive and mathematically simple procedure as may be preferred as per requirement 4). Any noise present on the image is amplified via division, with the frequencies which are present only weakly in the object suffering the worse noise amplification. A step artefact for example has a spectrum in which the amplitude falls off at higher frequencies, such that the inferred transfer function would be corrupted by noise to a greater extent at higher frequencies. At best a uniform object spectrum is therefore chosen, hence suggesting the use of large spherical objects or random arrays. Of these it is arguably the former which is practically easier to manufacture (requirement 5) within the tolerances demanded for industrial standards, however this has still to be realised in practice.

References

[1] D. J. Whitehouse. *Handbook of Surface Metrology*. IOP Publishing, Bristol and Philadelphia, 1994.

[2] R. K. Leach, editor. *Optical Measurement of Surface Topography*. Springer-Verlag Berlin, 2011.

[3] D. J. Whitehouse. Surface metrology. *Meas. Sci. Technol*, 8:955–972, 1997.

[4] R. Leach. *Fundamental principles of engineering nanometrology*. Elsevier, Amsterdam, 2009.

[5] G. Schmaltz. Über Glätte und Ebenheit als physikalisches und physiologisches problem. *Zeitschrift des Vereines deutcher Ingenieure*, 73:1461, 1929.

[6] S. Tolansky. *Surface microtopography*. Wiley Interscience, New York, 1960.

[7] J. M. Bennett. Measurement of the rms roughness, autocovariance function and other statistical properties of optical surfaces using a feco scanning interferometer. *Appl. Opt.*, 15:2705–2721, 1976.

[8] M. M. Miroshnikov. Academician Vladimir Pavlovich Linnik - The founder of modern optical engineering (on the 120th anniversary of his birth). *J. Opt. Technol.*, 77:401–408, 2010.

[9] B. Bhushan, J. C. Wyant, and C. L. Koliopoulos. Measurement of surface topography of magnetic tapes by mirau interferometry. *Appl. Opt.*, 24:1489–1497, 1985.

[10] K. Creath. Step height measurement using two-wavelength phase-shifting interferometry. *Appl. Opt.*, 26:2810–2816, 1987.

[11] B. S. Lee and T. C. Strand. Profilometry with a coherence scanning microscope. *Appl. Opt.*, 29:3784–3788, 1990.

[12] P. de Groot and L. Deck. Surface profiling by analysis of white-light interferograms in the spatial freqency domain. *J. Mod. Opt.*, 42:389–401, 1995.

[13] D. K. Hamilton and T. Wilson. Surface profile measurement using the confocal microscope. *J. Appl. Phys.*, 53:5320–5322, 1982.

[14] C. L. Giusca, R. K. Leach, F. Helery, T. Gutauskas, and L. Nimishakavi. Calibration of the scales of areal surface topography measuring instruments: Part 1 - Measurement noise and residual flatness. *Meas. Sci. Technol.*, 23:035008, 2011.

[15] C. L. Giusca, R. K. Leach, and F. Helery. Calibration of the scales of areal surface topography measuring instruments: Part 2 - Amplification, linearity and squareness. *accepted for publication in Meas. Sci. Technol.*, 2012.

[16] C. L. Giusca, R. K. Leach, F. Helery, and T. Gutauskas. Calibration of the geometrical characteristics of areal surface topography measuring instruments. *J. Phys.: Conf. Ser.*, 311:012005, 2011.

[17] R. K. Leach, C. L. Giusca, and K. Naoi. Development an characterisation of a new instrument for the traceable measurement of areal surface texture. *Meas. Sci. Technol.*, 20:125102, 2009.

[18] C. L. Giusca, R. K. Leach, and A. B. Forbes. A virtual machine-based uncertainty evaluation for a traceable areal surface texture measuring instrument. *Measurement*, 44:988–993, 2011.

[19] E. L. Church and P. Z. Takacs. Effects of optical transfer function in surface profile measurements. *Proc. SPIE*, 1164:46–50, 1989.

[20] P. de Groot and X. C. de Lega. Interpreting interferometric height measurements using the instrument transfer function. *Fringe*, pages 30–37, 2005.

[21] P. M. Duffieux. *Rennes*. L'integrale de Fourier et ses applications a l'Optique, 1946.

[22] E. W. H. Selwyn. *Photo. J.*, 88B:6–57, 1946.

[23] M. Gu, Gan. X., and C. J. R. Sheppard. Three-dimensional coherent transfer functions in fiber-optical confocal scanning microscopes. *J. Opt. Soc. Am. A*, 8:1019–1025, 1991.

[24] O. Nakamura and S. Kawata. Three-dimensional transfer-function analysis of the tomographic capability of a confocal fluorescence microscope. *J. Opt. Soc. Am. A*, 7:522–526, 1990.

[25] N. Streibl. Three dimensional imaging by a microscope. *J. Opt. Soc. Am. A*, 2:121–127, 1985.

[26] J. W. Goodman. *Introduction to Fourier Optics*. McGraw Hill, New York, 2nd edition, 1996.

[27] C. J. R. Sheppard and X. Q. Mao. Three dimensional imaging in a microscope. *J. Opt. Soc. Am. A*, 6:1260–1269, 1989.

[28] C. J. R. Sheppard and A. Choudhury. Image formation in the scanning microscope. *Opt. Acta*, 24:1051–1073, 1977.

[29] M. Gu. *Principles Of Three-Dimensional Imaging In Confocal Microscopes*. World Scientific, Singapore, 1996.

[30] M. Born and E. Wolf. *Principles of Optics*. Cambridge University Press, Cambridge, 7th edition, 1980.

[31] J. D. Jackson. *Classical Electrodynamics*. John Wiley & Sons, Ltd., New York, 1998.

[32] S. Trattner, M. Feigin, H. Greenspan, and N. Sochen. Validity criterion for the Born approximation convergence in microscopy imaging. *J. Micros. (Oxford)*, 124:107–117, 1981.

[33] C. W. McCutcheon. Generalised aperture and the three-dimensional diffraction image. *J. Opt. Soc. Am.*, 54:240–244, 1964.

[34] E. Wolf. Three-dimensional structure determination of semi-transparent objects from holographic data. *Opt. Commun.*, 1:153–156, 1969.

[35] B. R. Frieden. Optical transfer of the three-dimensional object. *J. Opt. Soc. Am.*, 57:56–66, 1967.

[36] H. H. Hopkins. On the diffraction theory of optical images. *Proc. R. Soc. London. Ser. A*, 217:408–432, 1953.

[37] H. H. Hopkins. The frequency response of a defocused optical system. *Proc. R. Soc. London. Ser. A*, 231:91–103, 1955.

[38] Sheppard C. J. R., D. K. Hamilton, and Cox. I. J. Optical microscopy with extended depth of field. *Proc. R. Soc. London. Ser. A*, 387:171–186, 1983.

[39] C. J. R. Sheppard and T. Wilson. Image formation in scanning microscopes with partially coherent source and detector. *Opt. Acta*, 25:315–325, 1978.

[40] C. J. R. Sheppard and T. Wilson. Fourier imaging of phase information in conventional and scanning microscopes. *Proc. R. Soc. London Ser. A*, 295:513–536, 1980.

[41] C. J. R. Sheppard and T. Wilson. The theory of the direct-view confocal microscope. *J. Micros. (Oxford)*, 124:107–117, 1981.

[42] T. Wilson and C. Sheppard. *Theory and Practice of Scanning Optical Microscopy*. Academic Press, London, 1984.

[43] C. J. R. Sheppard, M. Gu, and X. G. Mao. Three-dimensional coherent transfer function in a reflection mode confocal scanning microscope. *Opt. Commun.*, 25:281–284, 1978.

[44] C. J. R. Sheppard and M. Gu. Three-dimensional optical transfer function for an annular lens. *Opt. Commun.*, 81:276–280, 1991.

[45] M. Gu and C. J. R. Sheppard. Three-dimensional optical transfer function in the fibre-optical confocal scanning microscope using annular lenses. *J. Opt. Soc. Am. A*, 9:1991–1999, 1992.

[46] M. Gu and C. J. R. Sheppard. Three-dimensional coherent transfer function in reflection-mode confocal microscopy using annular lenses. *J. Mod. Opt.*, 39:783–793, 1992.

[47] M. Gu and C. J. R. Sheppard. Three-dimensional coherent transfer functions in confocal imaging with two unequal annular lenses. *J. Mod. Opt.*, 40:1255–1272, 1993.

[48] C. J. R. Sheppard, M. Gu, Y. Kawata, and S. Kawata. Three-dimensional transfer functions for high aperture systems. *J. Opt. Soc. Am. A*, 11:593–598, 1994.

[49] M. Gu and C. J. R. Sheppard. Effects of defocus and primary spherical aberration on three-dimensional coherent transfer functions in confocal microscopes. *Appl. Opt.*, 31:2541–2549, 1992.

[50] V. Drazic. Dependence of two- and three-dimensional optical transfer functions on pinhole radius in a coherent confocal microscope. *J. Opt. Soc. Am. A*, 9:725–731, 1992.

[51] D. Malacara, editor. *Optical Shop Testing*. Wiley-Blackwell, 3rd edition, 2007.

[52] P. Török and F.-J. Kao, editors. *Optical Imaging and Microscopy - Techniques and Advanced Systems*. Springer-Verlag, New York, 2 edition, 2007.

[53] G. J. Brakenhoff. Imaging modes in confocal scanning light microscopy. *J. Micros.*, 117:233, 1979.

[54] T. Wilson and R. Juškaitis. Scanning interference microscopy. *Bioimaging*, 2:36–40, 1994.

[55] J. Ojeda-Castañeda and E. Jara. Transfer function with quadratic detection: coherent illumination. *J. Opt. Soc. Am.*, 70:458–461, 1980.

[56] S. S. Kou and C. J. R. Sheppard. Imaging in digital holographic microscopy. *Opt. Express*, 15:13640–13648, 2007.

[57] S. S. Kou and C. J. R. Sheppard. Image formation in holographic tomography. *Opt. Lett.*, 33:2362–2364, 2008.

[58] J. Quartel and C. J. R. Sheppard. A surface reconstruction algorithm based on confocal interferometric profiling. *J. Mod. Opt.*, 43:591–605, 1996.

[59] M. Davidson, K. Kaufman, and I. Mazor. The coherence probe microscope. *Solid State Technol.*, 730:57–59, 1987.

[60] C. J. R. Sheppard, M. Roy, and M. D. Sharma. Image formation in low-coherence and confocal interference microscopes. *Appl. Opt.*, 25:1493–1502, 1978.

[61] M. Subbarao. Optical transfer function of a diffraction-limited system for polychromatic illumination. *Appl. Opt.*, 29:554–558, 1990.

[62] R. Barnden. Calculation of axial polychromatic optical transfer function. *Opt. Acta*, 21:981–1003, 1974.

[63] R. Barnden. Extra-axial polychromatic optical transfer function. *Opt. Acta*, 23:1–24, 1976.

[64] D. Navajas, S. Vallmitjana, J. J. Barandalla, and J. R. de F Moneo. Evaluation of polychromatic image quality by means of transfer function. *J. Opt.*, 13:283, 1982.

[65] B. Chakraborty. Polychromatic optical transfer function of a perfect lens masked by birefringent plates. *J. Opt. Soc. Am. A*, 5:1207–1212, 1988.

[66] P. de Groot and X. C. de Lega. Signal modelling for low-coherence height-scanning interference microscopy. *Appl. Opt.*, 43:4821–4830, 2004.

[67] J. M. Coupland and Lobera J. Holography, tomography and 3D microscopy as linear filtering operations. *Meas. Sci. Technol.*, 19:074012, 2008.

[68] Mitsuo Takeda. Chromatic aberration matching of the polychromatic optical transfer function. *Appl. Opt.*, 20:684–687, 1981.

[69] C. J. R. Sheppard and H. J. Matthews. Imaging by a high aperture optical system. *J. Opt. Soc. Am. A*, 40:1631–1651, 1993.

[70] C. J. R. Sheppard and M. Gu. Imaging by a high aperture optical system. *J. Mod. Opt.*, 40:1631–1651, 1993.

[71] C. J. R. Sheppard, J. N. Gannaway, and A. Choudhury. Electromagnetic field near the focus of wide-angular annular lens and mirror systmes. *Microwaves Opt. Acoust.*, 1:129–132, 1977.

[72] W. Urbaćzyk. Optical imaging in polarised light. *Optik*, 63:25–35, 1982.

[73] W. Urbaćzyk. Optical imaging systems changing the state of light polarization. *Optik*, 66:301–309, 1984.

[74] W. Urbaćzyk. Optical transfer functions for imaging systems which change the state of light polarization. *Opt. Acta*, 33:53–62, 1986.

[75] M. R. Arnison and C. J. R. Sheppard. A 3D vectorial optical transfer function suitable for arbitrary pupil functions. *Opt. Commun.*, 211:53–63, 2002.

[76] C. J. R. Sheppard and K. G. Larkin. Vectorial pupil functions and vectorial transfer functions. *Optik*, 107:79–87, 1997.

[77] C. J. R. Sheppard, T. J. Connolly, and M. Gu. Imaging and reconstruction for rough surface scattering in the Kirchoff approximation by confocal microscopy. *J. Mod. Opt.*, 14:2407–2421, 1993.

[78] P. Beckmann and A. Spizzichino. *The Scattering of Electromagentic Waves from Rough Surfaces*. Norwood, Mass. Artech, 1987.

[79] L. Baker, editor. *Selected papers on Optical Transfer Function: Foundation and theory*, volume MS 59 of *SPIE Milestone Series*. SPIE Opt. Eng. Press, Bellingham, 1992.

[80] L. Baker, editor. *Selected papers on Optical Transfer Function: Measurement*, volume MS 60 of *SPIE Milestone Series*. SPIE Opt. Eng. Press, Bellingham, 1992.

[81] E. L. Church, H. A. Jenkinson, and J. M. Zavada. Relationship between surface scattering and microtopographic features. *Opt. Eng.*, 18:125–136, 1979.

[82] E. L. Church and H. C. Berry. Spectral analysis of the finish of polished optical surfaces. *Wear*, 83:189–201, 1982.

[83] J. M. Elson and J. M. Bennett. Calculation of the power spectral density from surface profile data. *Appl. Opt.*, 34:201–208, 1995.

[84] V. V. Yashchuk, A. D. Franck, S. C. Irick, M. R. Howells, A. A. MacDowell, and W. R. McKinney. Two dimensional power spectral density measurements of x-ray optics with the micromap interferometric microscope. *Proc. SPIE*, 5858:58580A–1–12, 2005.

[85] G. Udupa, M. Singaperumal, R. S. Sirohi, and M. P. Kothiyal. Characterization of surface topography by confocal microscopy: I. principles and the measurement system. *Measu. Sci. Technol.*, 11:305–314, 2000.

[86] C. S. Williams and O. A. Becklund. *Introduction to the Optical Transfer Function*. SPIE Press, USA, 2002.

[87] S. K. Barber, E. D. Anderson, R. Cambie, W. R. McKinney, P. Z. Takacs, J. C. Stover, D. L. Voronov, and V. V. Yaschuk. Binary pseudo-random gratings and arrays for calibration of modulation transfer function of surface profilometers. *Nucl. Instr. Meth. A*, 616:172–182, 2010.

[88] D. A. Agard, Y. Hiraoka, P. Shaw, and J. W. Seday. Fluorescence microscopy in three dimensions. *Meth. Cell Biol.*, 30:353–377, 1989.

[89] S. F. Gibson and F. Lanni. Experimental test of an analytical model of aberration in an oil-immersion objective lens used in three-dimensional light microscopy. *J. Opt. Soc. Am. A*, 9:154–166, 1992.

[90] P. C. Goodwin. Evaluating optical aberration using fluorescent microspheres: methods, analysis, and corrective actions. *Methods Cell Biol.*, 81:397–413, 2007.

[91] Y. Hiraoka, J. W. Seday, and D. A. Agard. Determination of the three-dimensional behaviour in epifluorescence microscopy. *Biophys. J.*, 57:325–333, 1990.

[92] R. W. Cole, T. Jinadasa, and C. M. Brown. Measuring and interpreting point spread functions to determine confocal microscope resolution and ensure quality control. *Nat. Protocols*, 6:1929–1941, 2011.

[93] S. K. Rhodes, A. Barty, A. Roberts, and K. A. Nugent. Sub-wavelength characterisation of optical focal structures. *Opt. Commun.*, 145:9–14, 1990.

[94] J. L. Beverage, R. V. Shack, and M. R. Descour. Measurement of the three-dimensional microscope point spread function using a Shack Hartmann wavefront sensor. *J. Micros.*, 205:61–75, 2002.

[95] P. J. Lineberg. Measurement of contrast transmission characteristics in optical image formation. *Opt. Acta.*, 1:80–89, 1954.

[96] R. Barakat and A. Houston. Line spread function and cumulative line spread function for systems with rotational symmetry. *J. Opt. Soc. Am.*, 54:768–773, 1964.

[97] R. Barakat and A. Houston. Line spread and edge spread functions in the presence of off-axis aberrations. *J. Opt. Soc. Am.*, 55:1132–1135, 1965.

[98] S. Mallick. Measurement of optical transfer function with polarization inteferometer. *Opt. Acta.*, 13:247–253, 1966.

[99] K. G. Birch. A scanning instrument for the measurement of optical frequency response. *Proc. Phys. Soc.*, 27:901–912, 1961.

[100] M. D. Waterworth. A new method for the measurement of optical transfer functions. *J. Sci. Instrum.*, 44:195–199, 1967.

[101] P. Kuttner. An instrument for determining the transfer function of optical systems. *Appl. Opt.*, 7:1029–1033, 1968.

[102] B. Tatian. Method for obtaining the transfer function from the edge response function. *J. Opt. Soc. Am.*, 55:1014–1019, 1965.

[103] E. C. Yeadon. A comparison of two different methods of OTF measurement. *Appl. Opt.*, 8:2541–2544, 1969.

[104] P. Z. Takacs, M. X. Li, K. Furenlid, and E. L. Church. Step-height standard for surface profiler calibration. *Proc. SPIE*, 1995:235–244, 1993.

[105] E. Mainsah, W. Dong, and K. J. Stout. Problems associated with the calibration of optical probe based topography instruments. *Measurement*, 17:173–181, 1996.

[106] K. Hacking. An optical method of obtaining the frequency response of a lens. *Nature*, 181:1158–1159, 1958.

[107] J. Pouleau. Modulation transfer function measurement of optical systems in the visible and infra-red (5 to 20 μm) range. *Opt. Acta*, 22:339–346, 1975.

[108] A. Basuray and M. Shah. Optical-transfer-function evaluation utilizing a rotationally symmetric sinusoidal grating and a linear sinusoidal grating of finite height. *J. Opt. Soc. Am. A*, 8:212–216, 1991.

[109] E. Novak, C. Ai, and J. C. Wyant. Transfer function characterization of laser fizeau interferometer for high-spatial-frequency phase measurements. *Proc. SPIE*, 3134:114–121, 1997.

[110] G. D. Boreman and S. Yang. Modulation transfer function measurement using three- and four-bar targets. *Appl. Opt.*, 34:8050–8052, 1995.

[111] O. P. Nijhawan, P. K. Datta, and J. Bhushan. On the measurement of MTF using periodic patterns of rectangular and triangular wave forms. *Nouv. Rev. Opt.*, 6:33–36, 1975.

[112] S. T. Thurman. OTF estimation using a Siemens star target. In *Imaging Systems Applications*, page IMC5, 2011.

[113] M. C. Wood, X. Wang, B. Zheng, S. Li, W. Chen, and H. Liu. Using contrast transfer function to evaluate the effect of motion blur on microscope image quality. *Proc. SPIE*, 6857:68570F, 2008.

[114] H. Kubota and H. Ohzu. Method of measurement of response function by means of random chart. *J. Opt. Soc. Am.*, 47:666–667, 1957.

[115] A. Daniels, G. D. Boreman, A. D. Ducharme, and E. Sapir. Random transparency targets for modulation transfer function measurement in the visible and infrared regions. *Opt. Eng.*, 34:860–868, 1995.

[116] E. Levy, D. Peles, M. Opher-Lipson, and S. G. Lipson. Modulation transfer function of a lens measured with a random target method. *Appl. Opt.*, 38:679–683, 1999.

[117] C. Pieralli. Estimation of point-spread functions and modulation-transfer functions of optical devices by statistical properties of randomly distributed surfaces. *Appl. Opt.*, 35:8186–8193, 1994.

[118] W. Wittenstein, J. C. Fontanella, A. R. Newbery, and J. Baars. The definition of the OTF and the measurement of aliasing for sampled imaging systems. *Opt. Acta*, 29:41–50, 1982.

[119] S. K. Park, R. Schowengerdt, and M.-A. Kaczynski. Modulation-transfer-function analysis for sampled image systems. *Appl. Opt.*, 23:2572–2582, 1984.

[120] M. Marchywka and D. G. Socker. Modulation transfer function measurement technique for small pixel detectors. *Appl. Opt.*, 31:7198–7213, 1992.

[121] V. V. Yashchuk, W. R. McKinney, and P. Z. Takacs. Binary pseudo-random grating standard for calibration of surface profilometers. *Opt. Eng.*, 47:073602, 2008.

[122] S. K. Barber, P. Soldate, E. D. Anderson, R. Cambie, W. R. McKinney, P. Z. Takacs, D. L. Voronov, and V. V. Yashchuk. Development of pseudo-random binary gratings and arrays for calibration of surface profile metrology tools. *J. Vac. Sci. Tech. B*, 47:3213–3219, 2008.

[123] S. K. Barber, P. Soldate, E. D. Anderson, R. Cambie, S. Marchesini, W. R. McKinney, P. Z. Takacs, D. L. Voronov, and V. V. Yashchuk. Binary pseudo-random gratings and arrays for calibration of modulation transfer function of surface profilometers: recent developments. *Proc. SPIE*, 7448:744802, 2009.

[124] S. K. Barber, E. Anderson, R. Cambie, S. Marchesini, W. R. McKinney, P. Z. Takacs, D. L. Voronov, and V. V. Yashchuk. Stability of modulation transfer function calibration of surface profilometers using binary pseudo-random gratings and arrays with non-ideal groove shapes. *Opt. Eng.*, 49:053606, 2010.

[125] V. V. Yashchuk, W. R. McKinney, and P. Z. Takacs. Binary pseudo-random grating as a standard test surface for measurement of modulation transfer function of interferometric microscopes. *Proc. SPIE*, 6704:670408, 2007.

[126] V. V. Yashchuk, E. H. Anderson, S. K. Barber, N. Bouet, R. Cambie, R. Conley, W. R. McKinney, P. Z. Takacs, and D. L. Voronov. Calibration of the modulation transfer function of surface profilometers with binary pseudorandom test standards: expanding the application range to fizeau interferometers and electron microscopes. *Opt. Eng.*, 49:093604, 2010.

[127] G. C. Slyusarev. *Sov. J. Opt. Technol.*, 37:299–, 1970.

[128] V. V. Shymga. *Sov. J. Opt. Technol.*, 41:81–, 1975.

[129] S. Vallmitjana, D. Navajas, J. J. Barandalla, and J. R. de F. Moneo. A simple method of evaluating the polychromatic modulation transfer function for photographic systems. *J. Opt.*, 14:25–28, 1983.

[130] I. Juvells, S. Vallmitjana, D. Ros, and J. R. de F. Moneo. Numerical evaluation of the two-dimensional modulation transfer function by means of spot diagram. comparison with experimental measurements. *J. Opt.*, 14:293–297, 1983.

[131] M. Schrader, M. Kozubek, S. W. Hell, and T. Wilson. Optical transfer functions of 4pi confocal microscopes: theory and experiment. *Opt. Lett.*, 22:436–438, 1997.

[132] Y. Cotte, F. M. Toy, C. Arfire, S. S. Kou, D. Boss, I. Bergoënd, and C. Depeursinge. Realistic 3D coherent transfer function inverse filtering of complex fields. *Biomed. Opt. Express*, 2:2216–2230, 2011.

[133] H. H. Hopkins. Interferometric methods for the study of diffraction images. *Opt. Acta*, 2:23–29, 1955.

[134] J. L. Selligson. Phase measurement in the focal region of an aberrated lens. PhD thesis, 1981.

[135] R. Dändliker, I. Märki, M. Salt, and A. Nesci. Measuring optical phase singularities at subwavelength resolution. *J. Opt. A: Pure Appl. Opt*, 6:S189–S196, 2004.

[136] M. Schrader and S. W. Hell. Wavefronts in the focus of a light microscope. *J. Micros.*, 184:143–148, 1996.

[137] P. Török and F.-J. Kao. Point-spread function reconstruction in high aperture lenses focusing ultra-short laser pulses. *Opt. Commun.*, 213:97–102, 2002.

[138] Juškaitis R. and T. Wilson. The measurement of the amplitude point spread function of microscope objective lenses. *J. Micros.*, 189:8–11, 1997.

[139] J. N. Walford, K. A. Nugent, A. Roberts, and R. E. Scholten. High-resolution phase imaging of phase singularities in the focal region of a lens. *Opt. Lett.*, 27:345–347, 2002.

[140] A. Marian, F. Charriére, T. Colomn, F. Montfort, J. Kühn, P. Marquet, and C. Depeursinge. On the complex three-dimensional amplitude point spread function of lenses and microscope objectives: theoretical aspects, simulations and measurements by digital holography. *J. Microsc.*, 225:156–169, 2006.

[141] B. M. Hanser, M. G. L. Gustafsson, D. A. Agard, and J. W. Sedat. Phase-retrieved pupil functions in wide-field fluorescence microscopy. *J. Microsc.*, 216:32–48, 2004.

[142] H. M. Quiney, G. J. Williams, and K. A. Nugent. Non-iterative solution of the phase retrieval problem using a single diffraction measurement. *Opt. Express*, 16:6896–6903, 2008.

[143] U. W. Lee and L. J. Bond. Characterization of ultrasonic imaging systems using transfer functions. *Ultrasonics*, 31:405–415, 1993.

[144] R. Oppelt and H. Ermert. Transfer function analysis of a quasioptical ultrasonic imaging system. *Ultrason. Imag.*, 6:324–341, 1984.

[145] P. Zinin, W. Weise, and S. Boseck. Detection of the defocused transfer function of a confocal reflection acoustic microscope (SAM) by imaging of a step and a sphere. *Proc. SPIE*, 3581:347–358, 1998.

[146] W. Weise, P. Zinin, T. Wilson, A. Briggs, and S. Boseck. Imaging of spheres with the confocal scanning optical microscope. *Opt. Lett.*, 21:1800–1802, 1996.

[147] P. Zinin, W. Weise, O. Lobkis, and S. Boseck. The theory of three dimensional imaging of strong scatterers in scanning acoustic microscopy. *Wave Motion*, 25:213–236, 1998.

[148] P. Zinin, W. Weise, T. Zhai, G. A. D. Briggs, and S. Boseck. Determination of the defocused transfer function of a confocal reflection microscope by imaging of a sphere. *Optik*, 107:45–48, 1997.

[149] W. Weise, P. Zinin, A. Briggs, T. Wilson, and S. Boseck. Examination of the two dimensional pupil function in coherent scanning microscopes using spherical particles. *J. Acoust. Soc. Am.*, 104:181–191, 1998.

[150] C. R. Wolfe, J. D. Downie, and J. K. Lawson. Measuring the spatial frequency transfer function of phase-measuring interferometers for laser optics. *Proc. SPIE*, 2870:553–557, 1996.

[151] L. R. Baker. An interferometer for measuring the spatial frequency response to a lens system. *Proc. Phys. Soc. Lond. Ser. B.*, 68:871–880, 1989.

[152] P. Hariharan and D. Sen. A simple interferometric arrangement for the measurement of optical frequency response characteristics. *Proc. Phys. Soc. Lon.*, 75:434–438, 1960.

[153] D. Kelsall. *Proc. Phys. Soc. Lon.*, 73:465, 1959.

[154] A. J. Montgomery. Two methods of measuring optical transfer functions with an interferometer. *J. Opt. Soc. Am.*, 54:624–628, 1966.

[155] T. Tsuruta. Measurement of transfer functions of photographic objectives by means of a polarizing shearing interferometer. *J. Opt. Soc. Am.*, 53:1156–1160, 1963.

[156] D. Kelsall. Rapid interferometric technique for MTF measurements in the visible or infrared region. *Appl. Opt.*, 12:1398–1399, 1973.

[157] C. R. Mercer and K. Creath. Liquid-crystal point-diffraction interferometer. *Opt. Lett.*, 19:916–918, 1994.

[158] D. W. Griffin. Phase-shifting shearing interferometer. *Opt. Lett.*, 26:140–141, 2001.

[159] J. C. Wyant. A simple inteferometric MTF instrument. *Opt. Commun.*, 19:120–121, 1976.

[160] J. C. Wyant. OTF measurements with a white light source: an interferometric technique. *Appl. Opt.*, 14:1613–1615, 1975.

[161] F. T. Arecchi, M. Bassan, S. F. Jacobs, and G. Molesini. MTF measurement via diffraction shearing with optically superimposed gratings. *Appl. Opt.*, 18:1247–1248, 1979.

[162] C. P. Grover and H. M. van Driel. Autocorrelation method for measuring the transfer function of optical systems. *Appl. Opt.*, 19:900–904, 1980.

[163] G. Indebetouw. Some experiments in partially coherent imaging and modulation transfer function evaluation. *Appl. Phys. B*, 32:21–24, 1983.

[164] C. J. R. Sheppard. The spatial frequency cut-off in three dimensional imaging. *Optik*, 72:131–133, 1986.

[165] C. J. R. Sheppard. The spatial frequency cut-off in three dimensional imaging ii. *Optik*, 74:128–129, 1986.

[166] R. Mandal, K. Palodhi, J. Coupland, R. K. Leach, and D. Mansfield. Measurement of the point spread function in coherence scanning interferometry. *Proc. IConTOPII*, pages 252–257, 2011.

[167] K. Palodhi, J. Coupland, and R. K. Leach. Measurement of the point spread function in coherence scanning interferometry. *Proc. Int. Conf. Met. Props. Eng. Surf*, pages 119–203, 2011.

[168] P. D. Woolliams, R. A. Ferfuson, C. Hart, A. Grimwood, and P. H. Tomlins. Spatially deconvolved optical coherence tomography. *Appl. Opt.*, 41:2014–2021, 2010.

[169] P. D. Woolliams and P. H. Tomlins. Estimating the resolution of a commercial optical coherence tomography system with limited spatial sampling. *Meas. Sci. Technol.*, 22:065502, 2011.

[170] J. Chu, Q. Wang, J. P. Lehan, G. Gao, and U. Griesmann. Measuring the phase transfer function of a phase shifting interferometer. *Proc. SPIE*, 7064:7064C–1–8, 2008.